USING FORCE NETWORKS TO BETTER UNDERSTAND GRANULAR MATERIALS

by

JAMES SARTOR

A DISSERTATION

Presented to the Department of Physics
and the Division of Graduate Studies of the University of Oregon
in partial fulfillment of the requirements
for the degree of
Doctor of Philosophy

December 2021

DISSERTATION APPROVAL PAGE

Student: James Sartor

Title: Using Force Networks to Better Understand Granular Materials

This dissertation has been accepted and approved in partial fulfillment of the requirements for the Doctor of Philosophy degree in the Department of Physics by:

Ben McMorran	Chair
Eric Corwin	Advisor
Jayson Paulose	Core Member
Marina Guenza	Institutional Representative

and

Krista Chronister	Vice Provost for Graduate Studies

Original approval signatures are on file with the University of Oregon Division of Graduate Studies.

Degree awarded December 2021

DISSERTATION ABSTRACT

James Sartor

Doctor of Philosophy

Department of Physics

December 2021

Title: Using Force Networks to Better Understand Granular Materials

Force networks are an essential element to understanding the behaviors of jammed packings. As such, the Force Network Ensemble was formulated to describe the space of all possible force networks for a packing. In this work we study the Force Network Ensemble, showing that it is a versatile tool that can be used to learn more about jammed systems. We do so by demonstrating two new applications of the Force Network Ensemble, and additionally we examine scaling law prefactors, connecting mean field results with low dimensional jamming. In the first application, we use the Force Network Ensemble to calculate the entropy of a packing's force networks, concretely linking a microscopic measure with bulk themodynamic approaches. In the second, we use the Force Network Ensemble to predict contact changes in a packing under decompression. Finally, we show precision measurements of several jamming scaling laws, showing that mean field results are applicable for not just the scaling exponent, but also the prefactors.

This dissertation includes previously published and unpublished coauthored material.

CURRICULUM VITAE

NAME OF AUTHOR: James Sartor

GRADUATE AND UNDERGRADUATE SCHOOLS ATTENDED:

University of Oregon, Eugene, OR, USA
Auburn University, Auburn, AL, USA

DEGREES AWARDED:

Doctor of Philosophy, Physics, 2021, University of Oregon
Master of Science, Physics, 2017, University of Oregon
Bachelor of Science, Department of Physics, Physics, 2013, Auburn University

AREAS OF SPECIAL INTEREST:

Soft Condensed Matter, Jamming

PROFESSIONAL EXPERIENCE:

Graduate Employee, University of Oregon, 2016-2021

Software Developer, Performance Logic 2014-2015

Undergraduate Research Assistant, Auburn University 2011-2014

GRANTS, AWARDS AND HONORS:

Weiser Senior Teaching Assistant Award, UO Department of Physics, 2021

Outstanding Undergraduate Research Assistant, AU Physics Department, 2013

Undergraduate Research Fellow, Auburn University Office of the Vice President, 2012

PUBLICATIONS:

J. Sartor, and E.I. Corwin, "Predicting Defects in Soft Sphere Packings Near Jamming Using The Force Network Ensemble" *arxiv preprint* arXiv:2108.09385 (2021).

J. Sartor, S. A. Ridout, and E. I. Corwin, "Mean-Field Predictions of Scaling Prefactors Match Low-Dimensional Jammed Packings" *Phys Rev Letters* **126** (4) 048001 (2021)

J. Sartor and E. I. Corwin, "Direct measurement of force configurational entropy in jamming" *Phys Rev E* **101** (5) 050902 (2020)

D. Reedy, J. B. Williams, B. Gaire, A. Gatton, M. Weller, A. Menssen, T. Bauer, K. Henrichs, Ph. Burzynski, B. Berry, Z. L. Streeter, J. Sartor, I. Ben-Itzhak, T. Jahnke, R. Dörner, Th. Weber, and A. L. Landers, "Dissociation dynamics of the water dication following one-photon double ionization. II. Experiment" *Phys Rev A* **98** (5) 053430

C. W. McCurdy, T. N. Rescigno, C. S. Trevisan, R. R. Lucchese, B. Gaire, A. Menssen, M. S. Schöffler, A. Gatton, J. Neff, P. M. Stammer, J. Rist, S. Eckart, B. Berry, T. Severt, J. Sartor, A. Moradmand, T. Jahnke, A. L. Landers, J. B. Williams, I. Ben-Itzhak, R. Dörner, A. Belkacem, and Th. Weber, "Unambiguous observation of F-atom core-hole localization in CF_4 through body-frame photoelectron angular distributions" *Phys Rev A* **95** (1) 011401

A Menssen, C S Trevisan, M S Schöffler, T Jahnke, I Bocharova, F Sturm, N Gehrken, B Gaire, H Gassert, S Zeller, J Voigtsberger, A Kuhlins, F Trinter, A Gatton, J Sartor, D Reedy, C Nook, B Berry, M Zohrabi, A Kalinin, I Ben-Itzhak, A Belkacem, R Dörner, T Weber, A L Landers, T N Rescigno, C W McCurdy and J B Williams, "Molecular frame photoelectron angular distributions for core ionization of ethane, carbon tetrafluoride and 1,1-difluoroethylene" *J Phys B* **49** (5) 055203

ACKNOWLEDGEMENTS

Full acknowledgement of all the support I've received through the writing of this would be longer than the dissertation itself. Nevertheless, I'd like to take a moment to express my gratitude here to those who have contributed the most to this work.

First and foremost I would like to thank my advisor Eric Corwin for his unwavering support over the past five years. Without your enthusiasm, expertise, and flexibility, this would not have been possible.

I am grateful as well for the excellent labmates that I have had here, for myriads of help and support: Cam Dennis, Francesco Arceri, Varda Faghir Hagh, Andy Hammond, Valerie Beale, Aileen Carroll-Godfrey, Jack Dale, Nicole Wales, Jacob Hass, Alex Trevelyan, Georgios Tsekenis, and Mike van der Naald.

Special thanks to Sean Ridout for not only the contributions to the letter which we wrote together, but also for providing insightful feedback on my other projects. I would also like to acknowledge Francesco Zamponi for graciously elucidating mean field results for us.

Thanks to Peter Morse for advice on both research and death cults. I would also like to acknowledge my committee for their advice and support throughout this process.

Lastly I would like to thank all my friends and family for their support, as well as innumerable fellow grad students, faculty, and staff who have helped me in various ways through this time.

This work was supported by the NSF Career Award grant No. DMR-1255370, and the Simons Collaboration on Cracking the Glass Problem (No. 454939 E. Corwin)

TABLE OF CONTENTS

LIST OF FIGURES

CHAPTER I

INTRODUCTION

Anyone who has stacked oranges knows that it is easy and intuitive to stack them closely in a dense lattice, as demonstrated in figure 1(a). Filling about 74% of space, the close packed lattice is in fact the densest possible arrangement of equal sized spheres in 3 dimensions. This was originally conjectured by Kepler in 1611 [1], but was not formally proven until 1998 [2]. If one simply pours them together, they will instead arrange themselves in an amorphous (i.e. random) and less dense structure, as shown in figure 1(b). This amorphous configuration is significantly less efficient, filling only about 64% of space. The lazy but innovative produce worker may attempt to create a close lattice by randomly pouring oranges into a box and squeezing, but experience dictates that this is impossible. The fruit are too much in each other's way to rearrange and relieve the stress from the squeezing. Interestingly, 2 dimensional discs of equal size do spontanously form hexagonal lattices when squeezed, but even discs of nonuniform size generally become frustrated and arrange amorphously.

Granular materials are collections of distinct macroscopic objects, such as sand, ball bearings, or piles of oranges. While crystalline structures such as close lattices are relatively straightforward to understand and analyze, the random features of amorphous granular systems make them extremely difficult to understand from first principles. The only analytic approach

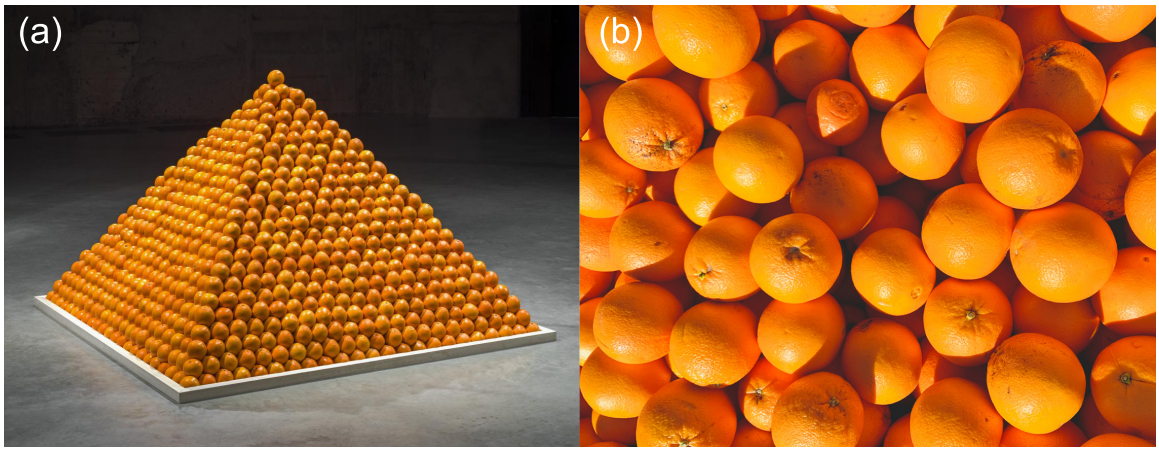

FIGURE 1. Left, stack of oranges constructed in a close packed lattice [3]. Right, oranges arranged amorphously [4].

that has been somewhat successful requires taking the limit of infinite spatial dimensions, termed "mean field." Since all physical systems are finite dimensional, results from the mean field limit do not necessarily apply. Many results from the mean field are however surprisingly accurate even in as low as 2 and 3 dimensions. Our research is not focused on analytic theory, but rather on computational study of soft spheres, i.e. spheres which are able to interact with their neighbors, imparting variable forces upon them. In general when one simulates systems in greater than three dimensions, the purpose is to draw parallels with results from the mean field.

A phase transition is when a material undergoes a discontinuous change in some property (the "order parameter") as some other property (the "control parameter") varies. The most well known phase changes are freezing/melting and boiling/condensing, for which the temperature is the control parameter, and the density of the material can be seen to discontinuously change at critical temperatures. The order parameter is generally accepted to be the free energy - at the phase transition, melting absorbs a latent heat in addition the heat required just to heat it to the melting point. While glasses go through thermal phase transitions, granular materials do not, because thermal fluctuations are insufficient in scale to allow rearrangement of grains. For example, take the box of oranges discussed earlier: thermal fluctuations (providing energy $E \sim kT \sim 0.026$ eV) cannot cause a pair of oranges to rearrange (requiring $E \sim mgh \sim 10^{17}$ eV). Granular materials are thus described as "athermal" or "zero-temperature." Granular materials do however go through a different type of transition, called the jamming and unjamming transitions, which are somewhat analogous to thermodynamic phase transitions. The control parameter for the jamming transition is the fraction of space occupied by particles, or packing fraction φ, and the jamming transition happens at a critical packing fraction φ_J, where properties of the system go through discontinuous changes. In particular, the pressure P begins to increase from 0, and the number of force bearing contacts between granules goes from 0 to roughly the number of particles times the spatial dimension Nd. The critical packing fraction is an exact value for any particular system, but generally has some variation between systems, and can vary based on the protocol of system generation. The jamming point can be understood as a critical point, and as the system increases in packing fraction from that point, properties such as the number of contacts in excess of Nd, the pressure, and the packing fraction in excess of φ_J all scale with each other as power laws [5, 6].

Traditional approaches to analyzing thermodynamic systems rely on the assumption of ergodicity, i.e. that the thermal system explores the ensemble of all available configurations. The probability of existing in any particualar configuration is determined by the ratio of the energy of that configuration with the temperature of the system. In a zero temperature granular material, however, this is obviously impossible. Despite this, granular materials do respond predictably to repeated disturbances, e.g. if you repeatedly shake a box of rocks, they will reliably settle into a configuration of roughly the same packing fraction. Thus, some version of athermal statistical mechanics is clearly at work. In 1989 Sam Edwards began a systematic attempt at understanding granular materials in thermodynamic terms [7]. "Angoricity," which relates entropy to pressure rather than energy is derived from this work and has shown promise as a temperature analog for granular materials [8, 9].

The jamming transition identifies the onset of rigidity. Below φ_j, a system is floppy and unable to sustain any force. Above φ_j however a system becomes rigid and can support external forces. You can run your hands through sand at the beach, but if you compress it, it will push back. This rigidity can be understood in terms of degrees of freedom and constraints - it arises when the system has at least as many constraints as degrees of freedom. A system where these are exactly equal is termed "isostatic," and a system with more constraints than degrees of freedom is termed "hyperstatic." Since each particle can move in d dimensions, a granular system has Nd degrees of freedom. The constraints on those degrees of freedom are the contacts between particles, which increase in quantity with increasing packing fraction or pressure. The jammed configurations under inquiry are hyperstatic and thus are rigid and may support external forces. When considering instead the force network of the system, each contact is a degree of freedom, and requiring force balance on each particle imposes Nd constraints. Thus while the positions of particles in a hyperstatic system is overdetermined, the force network supporting this rigidity is underdetermined. There exists a degerate space of allowed force configurations, which is referred to as the Force Network Ensemble or FNE [10, 11]. This Force Network Ensemble framework forms the basis for the majority of the material in this work.

The following three chapters are the three first author papers which I composed during my time as a graduate student. Chapter II (published in PRE [12]) explores a method that I developed along with Eric Corwin that uses the Force Network Ensemble to measure the allowed

space of force configurations for a granular system. This allowed us to measure the entropy of the force networks for the first time from the microscopic structure. We confirm this entropy measurement by comparing it with a bulk measurement of angoricity, concretely linking it with the microscopic multiplicity of the Force Network Ensemble. In Chapter III (in review [13]), we use a similar approach to examine the boundaries of the allowed space of force configurations. These boundaries correspond to systems with fewer contacts than the original system. By examining which contacts are missing in those boundary systems, we are able to predict which contacts between particles are unnecessary. We then show that only these defect contacts may in fact be broken under decompression. These force network defects are a completely new form of defect in amorphous materials. In chapter IV (published in PRL [14]), working with Eric Corwin and Sean Ridout, we closely examine the relation between critical scaling laws about the jamming transition. Rather than just looking at the well known exponents of these scaling laws, we delve deeper and explore the prefactors to these scaling laws. Although pefactors such as these are generally highly sensitive to finite dimensional corrections, we show that they are still well predicted by the mean field. We provide a first principles proof for one free of the mean field assumption, demonstrating that mean field theory is not necessary for explaining scaling laws in low dimensional jamming.

CHAPTER II

DIRECT MEASUREMENT OF FORCE CONFIGURATIONAL ENTROPY IN JAMMING

Introduction

Thermodynamics connects abstract and difficult to measure details, such as entropy, with more easily measured bulk properties, such as temperature. In granular systems, for which the thermal energy scale is irrelevantly small, similar connections have been proposed for the volume ensemble [7, 9] using compactivity as a temperature analog and also for the force network ensemble [8, 9] using angoricity. While these quantities are measurable [15, 16], they are not physically meaningful unless they 1) are shown to have temperature-like properties, such as following the zeroth law and 2) can be rigorously linked to a first principles definition of microscopic entropy [17]. Entropy itself was initially an empirical quantity until Sackur and Tetrode placed it on firm footing for the ideal gas with the discretization of phase space into quantum mechanical states [17, 18]. The length scale of the discretization depends both on properties of the system and the universal constant $\hbar$, whose value cannot be inferred from bulk properties of the ideal gas alone. Angoricity holds promise as a temperature analog, as it has been shown to follow the zeroth law, while compactivity fails to do so [9, 15, 19]. However, before the thermodynamic approach of angoricity can be considered to be on solid ground, the nature of the entropy of jammed systems must first be understood.

When the density of an overjammed packing increases, force networks are affected in two ways: 1) force magnitudes, and thus pressure, increase, and 2) new contacts between particles form, increasing the number of contact forces in the network. Both of these changes increase the entropy of the force networks. While the effect on entropy from pressure changes is well understood [16, 20], the effect from changes in the contact network is not. To decouple these effects, we propose an extension to the Force Network Ensemble in which changes in the contact network are allowed. This leads us to identify a critical number of excess contacts, δz_c, describing the transition from a regime in which entropy is dominated by changes in pressure to one in which it is dominated by changes in the contact network.

The temperature analogue angoricity is defined as the derivative of entropy with respect to the stress tensor [8]. In isotropic systems this tensor quantity can be simplified to a scalar

derivative of entropy with respect to pressure. Just as temperature of an ideal gas can be measured from the velocity distribution, angoricity can be measured from the distribution of local pressures [16]. As a derivative, angoricity provides information about the difference in entropy between two systems but not the absolute values. Previous theoretical and experimental work has identified an inverse scaling of angoricity with pressure in the near jamming limit for two-dimensional (2D) soft spheres [16, 20]. However, these studies do not systematically explore the effect of changing the contact network, which remains static in the near jamming limit. In our computational study, we explore the system by varying the spatial dimension, pressure, and number of particles over ranges much larger than would be feasible in a physical experiment.

In this Rapid Communication, we present a first principles derivation of the entropy for the force networks of granular packings. We measure this entropy up to a multiplicative constant, h_f, in the near jamming limit by directly measuring the volume of the space of allowed force configurations. Analogous to Planck's constant in the Sackur-Tetrode equation, h_f discretizes the space of force configurations into an integer number of accessible states. We then use the method of overlapping histograms to measure angoricity as a function of pressure, and compare with our force volume measure to solve for h_f. This concretely connects the bulk nature of angoricity with the microscopic multiplicity of the force network ensemble.

Computational methods

We use pyCudaPacking [21], a GPU-based simulation engine, to generate energy minimized soft sphere packings at specified pressures in periodic boundary conditions. We do so for number of particles, N, spanning from 256 to 4096, and dimension, d, from 2 to 5. The particles are monodispersed, except in 2D in which we use equal numbers of bidispersed particles at a size ratio of 1.4:1 to prevent crystallization. Particles interact through a harmonic contact potential as defined in [21], and the system's energy is minimized using the FIRE minimization algorithm [22].

Starting with random initial positions, we minimize energy and then adjust overall density by uniformly scaling particle radii to achieve a pressure P of 10^{-2} in natural units, as defined in [5]. This pressure is chosen to prevent crystallization artifacts from high density packings. From there, we iteratively adjust the density both up and down to achieve specific values of pressure. We do this efficiently by exploiting the known linear scaling of pressure with density

above jamming for a harmonic potential [6]. For each targeted pressure, we ensure that the actual pressure is accurate to a factor of 10^{-5}. We sample 100 logarithmically spaced steps per decade of pressure to ensure sufficient overlap between the distributions of local pressure for neighboring systems, as is needed for the method of overlapping histograms.

Rigidity

To understand the behavior of packings close to the jamming transition we examine the geometric mechanisms necessary for rigidity by constructing an unstressed spring network with the geometry of the packing. The rigidity matrix [23–25], $\mathcal{R}$, describes this spring network by encoding the normalized contact force vectors from the packing, n_{ij}, between pairs of particles i and j as

$$\mathcal{R}^{k\alpha}_{\langle ij \rangle} = (\delta_{jk} - \delta_{ik}) n^{\alpha}_{ij}, \tag{2.1}$$

where k indexes contacts and α indexes spatial dimensions. For a system with N_{stable} stable particles and N_{contact} contacts, this will be an N_{contact} by $N_{\text{stable}}d$ matrix. The singular value decomposition of this matrix yields two sets of singular vectors, analogous to eigenvectors for a square matrix. The right singular vectors describe the normal modes of position displacements, and the left singular vectors describe the normal modes of force displacements. The left singular vectors corresponding to zero eigenvalues represent mechanically stable force configurations, termed states of self stress. These vectors need not be positive definite, and therefore are not necessarily valid force configurations for the underlying packing.

The magnitude of each contact force can be considered as a degree of freedom while the requirement for mechanical stability introduces d constraints for each particle. Balancing these constraints requires a minimum number of contacts to ensure stability, which in systems with periodic boundary conditions is given by [26, 27]

$$N^{\text{min}}_{\text{contact}} = d(N_{\text{stable}} - 1) + 1. \tag{2.2}$$

A system with this minimum number of contacts has exactly one state of self stress, and each additional contact formed imparts an additional independent state of self stress. Thus, we define

the number of excess contacts, ΔZ as

$$\Delta Z = N_{\text{contact}} - N_{\text{contact}}^{\text{min}}, \tag{2.3}$$

making the number of independent states of self stress $\Delta Z + 1$. We define the number of excess contacts per particle,

$$\delta z = 2\Delta Z/N, \tag{2.4}$$

where the 2 reflects that each excess contact is shared between two particles. These independent states of self stress form a basis for the $\Delta Z + 1$ dimensional space of all mechanically stable force configurations of the spring network. However, imposing a normalization condition restricts this to a ΔZ dimensional subspace.

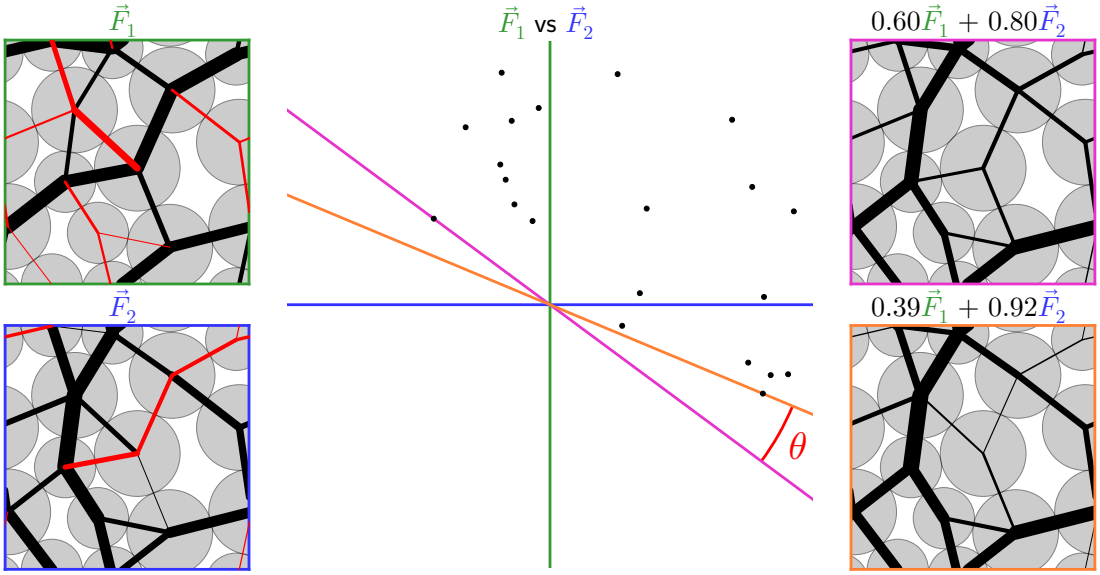

FIGURE 2. Force volume measurement for a system with one excess contact. Left, the two independent states of self stress, F_1 and F_2. Black lines between particles represent positive (compressive) forces, red lines represent negative (tensile) forces. Center, a scatter plot of F_1 vs F_2 for each pair of particles. Linear combinations of F_1 and F_2 are represented graphically by drawing a sloped line through the origin and measuring the distance to each point. Any sloped line for which all of the points fall into the same half-space corresponds to a positive definite linear combination. The set of lines which allow for such solutions is the force space volume, indicated by the angle θ. Note that in a system with ΔZ excess contacts, this volume is a ΔZ dimensional quantity. Right, the two extremal positive-definite linear combinations at the edge of this region are shown. Each has one force brought to precisely zero.

Force Volume

The force network ensemble samples all valid force networks in the spring representation of a packing with equal probability [10, 11, 28]. To determine the force volume, we calculate the normalized independent states of self stress where F_μ^q is the contact force on contact q in the state of self stress μ. The set of all possible repulsive contact forces is defined by linear combinations that satisfy

$$\sum_\mu \lambda_\mu F_\mu^q \geq 0 \tag{2.5}$$

for all contacts q, where $\{\lambda_\mu\}$ are coefficients subject to the normalization condition $\sum_\mu \lambda_\mu^2 = 1$. We define the force volume V_f to be the volume of the space of λ_μ coefficients that satisfy this rule as illustrated in Fig. 2.

We measure this force volume with the following protocol:

1. Recast F_μ^q into a set, $\{\vec{C}^q\}$, of N_{contacts} vectors containing the value of the force on contact q in each of the $\Delta Z + 1$ states of self stress.

2. Planes which pass through the origin and place all of the $\{\vec{C}^q\}$ into a single half-space satisfy inequality (2.5). We compute the extremal values of such planes as the facets of the convex hull [29] of $\{\vec{C}^q, \vec{0}\}$. The normal vector to each facet is the $\{\lambda_\mu\}$ which defines a vertex of the allowed space of coefficients and corresponds to a linear combination of the independent states of self stress in which exactly ΔZ forces are precisely 0.

3. To respect the normalization requirement we calculate V_f as the ΔZ dimensional solid angle subtended by the volume defined by these vertices in coefficient space.

We convert this volume into a pure number of configurations by discretizing it into hypercubes of side length h_f, named to emphasize the parallelism with Planck's constant h used in the enumeration of phase space states in the Sackur-Tetrode equation. Because the pressure sets the scale of the average force, we then multiply this enumeration by the pressure, as has been shown in previous theoretical and experimental work [16, 20, 30]. Putting these considerations together, we arrive at an ansatz relating the microscopic force volume to the multiplicity, and thus

the entropy:

$$\Omega = P\frac{V_f}{(h_f)^{\Delta Z}} \qquad \Longrightarrow \qquad S = \ln P + \ln V_f - \Delta Z \ln h_f. \tag{2.6}$$

Although pressure and number of excess contacts both appear in the entropy, they are not independent variables but related in the thermodynamic limit by [5, 6]

$$\Delta Z = B(d)N\sqrt{P}. \tag{2.7}$$

where B is some function of dimension only. We find values of B of approximately 2.1, 6.0, 12.5, and 23 in dimensions two, three, four, and five. These values are roughly consistent with previous studies for two and three dimensional spheres [5, 27].

Angoricity [8], α, is derived as:

$$\alpha \equiv \frac{\partial S}{\partial P} = \frac{1}{P} + \frac{\partial}{\partial P}\ln V_f - \frac{1}{2}\frac{BN}{\sqrt{P}}\ln h_f. \tag{2.8}$$

First, we measure the volume of force space V_f and explore how it scales with the number of excess contacts. Second, we measure bulk angoricity to confirm our prediction in Eq. (2.8) and measure the microscopic constant h_f.

Results

As shown in Fig. 3, the measured force volume scales exponentially with the number of excess contacts:

$$V_f \;=\; C\gamma^{\Delta Z}. \tag{2.9}$$

We find C to be well approximated by 1, as shown in the top inset. The lower inset shows that γ decreases with increasing N and d.

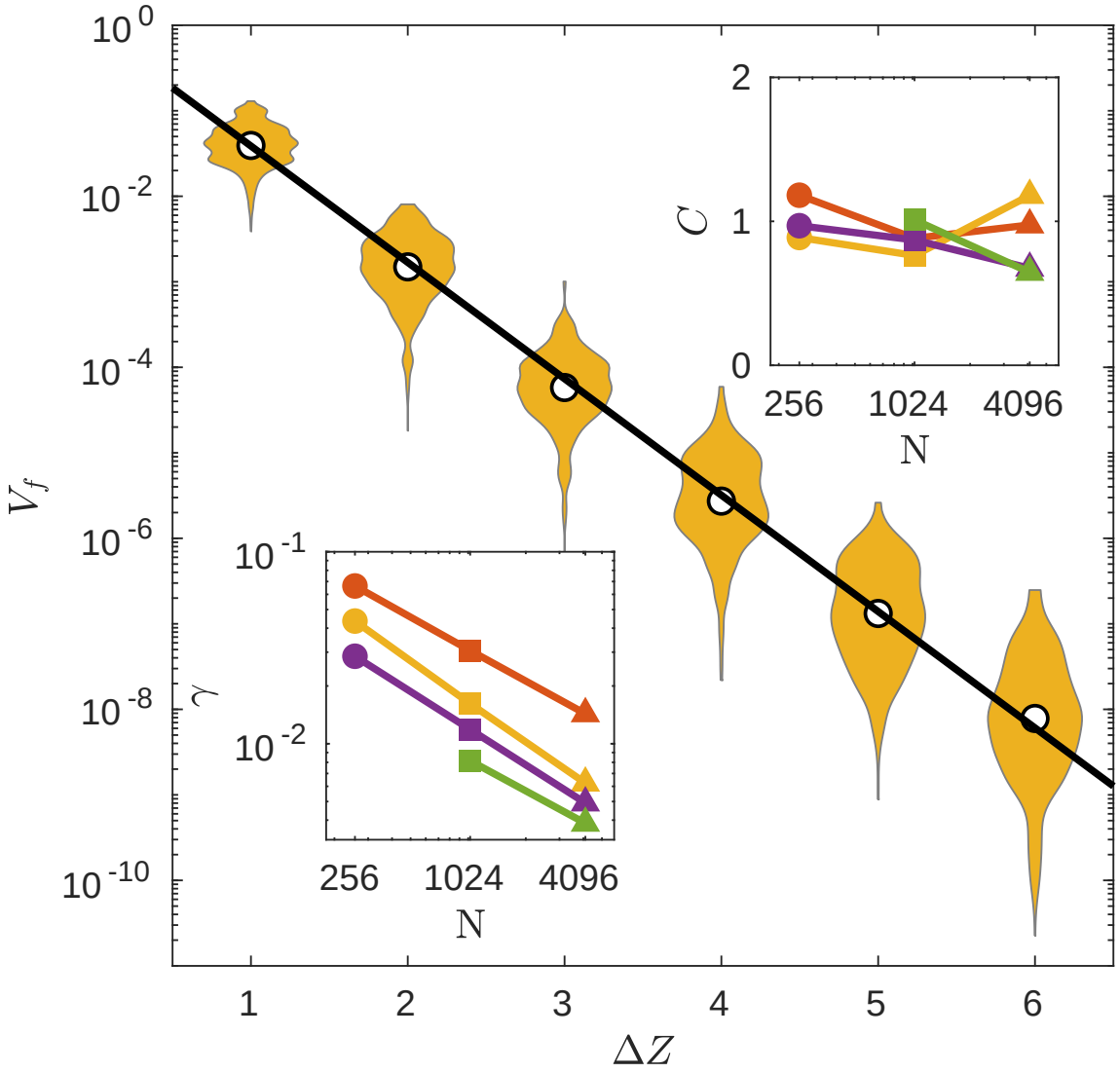

FIGURE 3. Representative exponential scaling of the force volume, V_f, with number of excess contacts, ΔZ, for $N = 1024$, $d = 3$. The median of the distribution for each ΔZ is shown as a white circle, surrounded by the full distribution in yellow. The black line shows the exponential fitting form, with exponential base γ. Inset bottom left, γ for each N and d. Inset top right, the scale, C of the exponential. Inset data is presented for $d = 2$ (red), 3 (yellow), 4 (purple), and 5 (green), and $N = 256$ (circles), 1024 (squares), and 4096 (triangles).

We can simplify the expression for angoricity by combining the preceding three equations to find

$$\alpha = \frac{1}{P} + \frac{1}{\sqrt{P_c P}} \tag{2.10}$$

where the crossover pressure between the two power laws is

$$P_c = \left[\frac{BN}{2} \ln \left(\frac{\gamma}{h_f} \right) \right]^{-2}. \tag{2.11}$$

We use the method of overlapping histograms of local pressures [16, 31, 32] to measure angoricity and determine the value of P_c and therefore h_f. For each system, we measure the local pressure for many random samples of a particle with its $m = 50$ nearest neighbors. The choice of m controls the sharpness of the local pressure distribution and so induces a trivial prefactor A, shown in the inset to Fig. 4 to be proportional to dm. We then compute the angoricity by comparing these local pressure distributions as in Ref [16]. We fit the angoricity curve to the power law in Eq. (2.10) with prefactor A and an additive offset. As shown in Fig. 4, all data collapse onto Eq. (2.10). We extract the crossover pressures, P_c, shown in the upper inset of figure 4, and find that they are insensitive to N, but decrease with increasing d.

Discussion

From Eq. (2.11) and our measured values of γ and P_c we compute h_f, shown in the inset to Fig. 5. A complete expression for entropy can now be written as

$$S = \ln P + \Delta Z \ln \left(\frac{\gamma}{h_f} \right). \tag{2.12}$$

This can be recast into a natural form using equations (2.7) and (2.10) by expressing the ratio of γ and h_f as a critical number of excess contacts per particle,

$$\delta z_c = 2B\sqrt{P_c} = \frac{2}{N \ln \left(\frac{\gamma}{h_f} \right)} \tag{2.13}$$

$$S = \ln P + \frac{\delta z}{\delta z_c}. \tag{2.14}$$

Thus, the entropy is dependent on two intensive thermodynamic variables, P and δz, and a constant δz_c for each dimension. While h_f is observed to decrease with N and expected to vanish in the thermodynamic limit, we find δz_c to be intensive with system size, as shown in Fig. 5.

The first term in Eq. (2.14) describes the entropy increasing from the absolute pressure scale, whereas the second describes the entropy increasing from the number of contacts increasing.

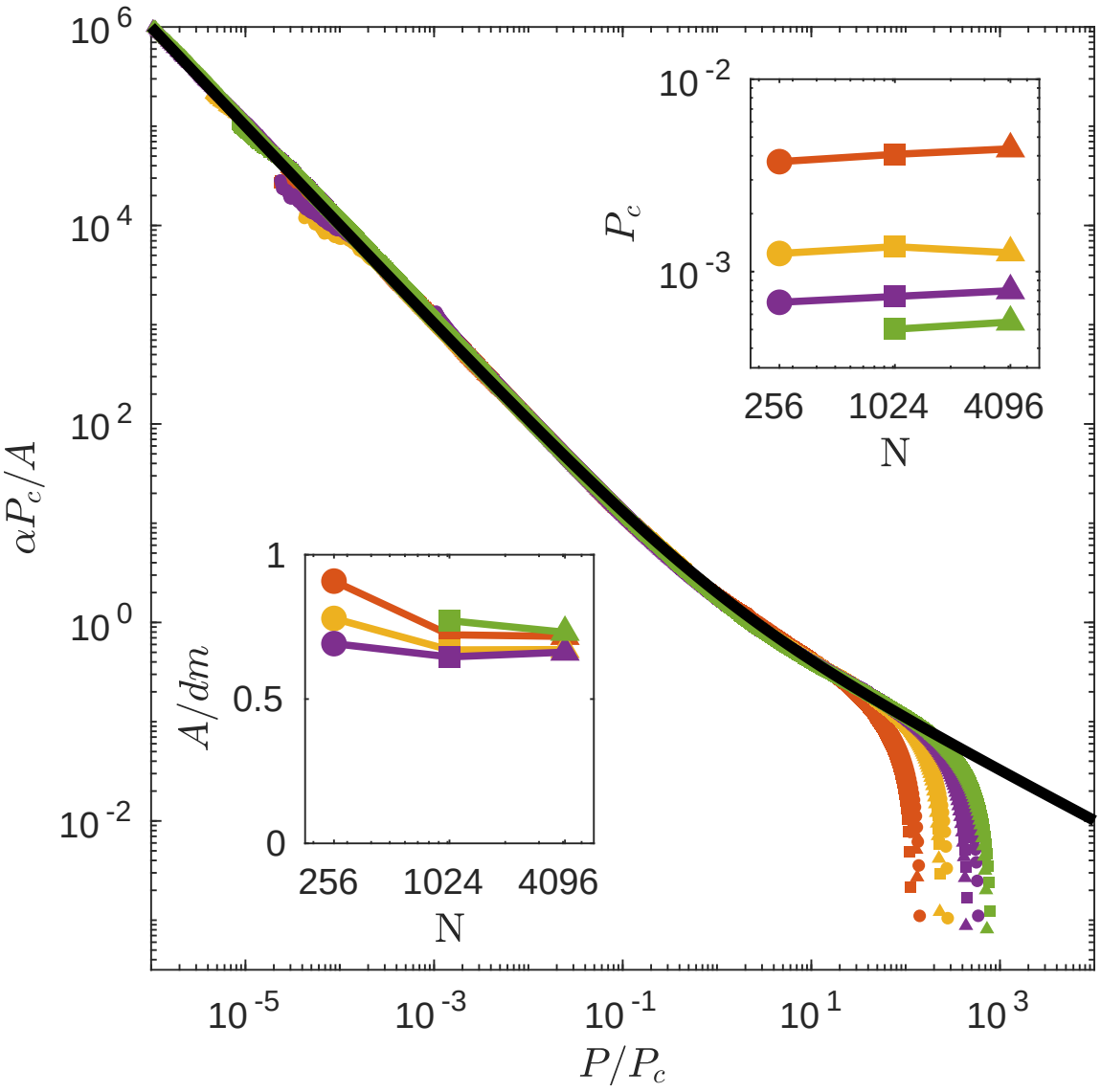

FIGURE 4. Scaled angoricity, $\alpha P_c/A$, for all N and d, collapses onto equation 2.8 (black line) when plotted against scaled pressure, P/P_c, until high pressure deviations caused by second nearest neighbor interactions. Inset top right, the crossover pressure P_c. Inset bottom left, A/dm is approximately 0.7. Colors denote dimension from 2-5 and symbol denotes number of particles as in figure 3.

Sufficiently close to jamming the first term will dominate as there will be few changes in the contact network even as the pressure changes dramatically. Further from jamming the second term will dominate, reflecting the primacy of changes in the contact network. Note that while this equation may be rewritten as a function of pressure using Eq. (2.7), for any particular finite packing the integer number of excess contacts is required to calculate the entropy precisely.

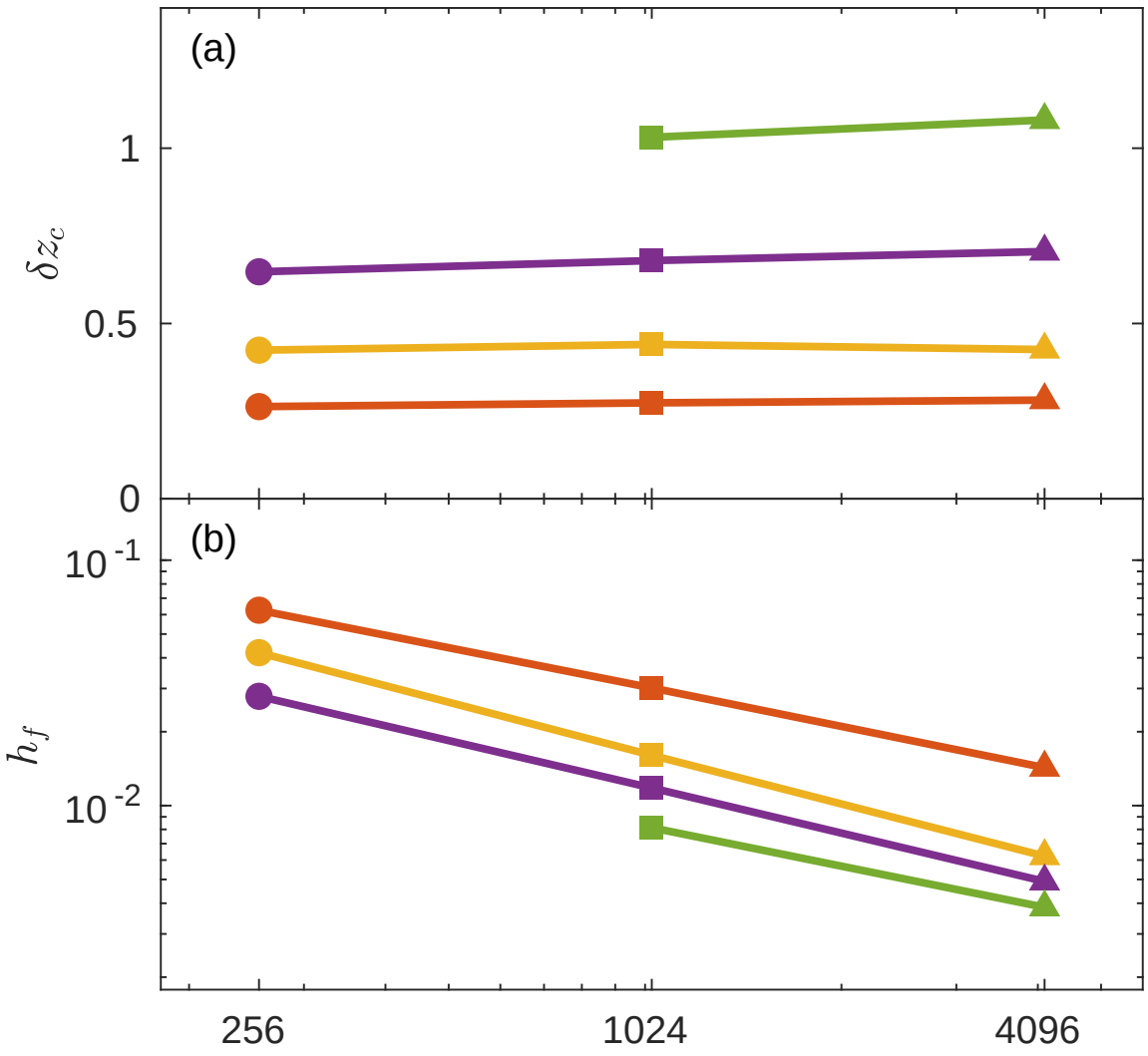

FIGURE 5. Upper, scaling of δz_c with N and d. Lower, scaling of h_f, with N and d, calculated from P_c by inverting equation 2.11. Colors denote dimension from 2-5 and symbol denotes number of particles as in figure 3.

Conclusion

We have demonstrated that the force network ensemble framework can be used to directly compute the multiplicity of the force configurations in packings close to the critical jamming point. We have presented an ansatz linking the volume of the force configurational space associated with a packing to the entropy of the packing. This entropy can be expressed as a function of pressure and is independently confirmed by measurements of the angoricity over approximately seven orders of magnitude of pressure. We have combined these two approaches

of measuring entropy in order to extract the fundamental scales governing the discretization of phase space that allows for enumeration. We discover a crossover value for the excess contacts per particle, δz_c, below which the entropy is governed primarily by changes in pressure at fixed contact network and above which the entropy is governed primarily by the creation of new contact forces.

This work places angoricity on a firm footing as a thermodynamic quantity that controls the behavior of overjammed systems. By tracing this entropy all the way down to an enumeration of states we discover that, perhaps unsurprisingly, Planck's constant does not set the fundamental scale of discretization h_f. In a purely classical model such as this, the discretization can only depend on the finite size effects of the system which are determined by N and d. Thus, in the thermodynamic limit, while h_f vanishes, the behavoir of the system is controlled by δz_c and thus P_c which do obtain fixed values. This full expression for entropy provides the first concrete linking of the microscopic force network ensemble to the thermodynamic description of granular materials and offers a complete description for the thermodynamics of the force networks in overjammed systems.

CHAPTER III

PREDICTING DEFECTS IN SOFT SPHERE PACKINGS NEAR JAMMING USING THE FORCE NETWORK ENSEMBLE

Introduction

From crafting swords and arrowheads in antiquity to perusing katanas at the mall today, choosing the available materials with highest strength has always been of critical concern. It is the weak points, and modes of failure, that determine the strength of a material. In polycrystalline materials these weak points arise from defects in the crystal structure [33]. Early approaches to amorphous systems attempted to model them as highly defective crystalline systems, but such models fail to capture emergent phenomena [34]. Amorphous systems thus must be treated in their own right, consequently there exists no obvious definition of a defect. However, "soft spots" can be found which are locations in which rearrangements are more likely to occur under shear. These were first explored via analysis of the low-frequncy quasilocalized vibrational modes [35] and have been more recently identified by using machine learning analysis on the local structure [36–44]. While this has been highly effective at identifying sites of rearrangements under shear, it has not been applied to systems under decompression, another common failure mode of materials. More importantly, while softness is correlated with structural quantities such as local potential energy and coordination number, these structural properties are not good predictors of rearrangements on their own. Thus softness, while useful as a heuristic, lacks analytic clarity. Additionally, while softness is an excellent predictor of instabilities, it does not predict stable contact network changes (i.e. contact changes which do not result in rearrangements), which comprise the majority of contact network changes [45, 46]. In this work we demonstrate a method for identifying defective contacts under decompression asymptotically close to the jamming/unjamming transition. We use the geometry of the force network ensemble to show that in the near-jamming limit there exists only a small and precisely identifiable number of contacts at which any contact network change can occur.

Background

To achieve mechanical stability, any system must have at least as many constraints as degrees of freedom. In a granular system, these constraints are borne by the contacts, and for a d dimensional system of frictionless spheres, the minimum number of contacts $N_c^* \sim Nd$ [47]. Any system that posseses more than this minimum number of contacts will have a resultant indeterminacy in its force networks as there must exist multiple linearly independent solutions for force balance. Near jamming, the overlaps (or deformations) between particles are much smaller than the interparticle distances. Due to this separation of scales, the forces in a system can be decoupled from the particle positions, and therefore can be considered to be a random instantiation within the space of the force indeterminancy [10–12, 28]. This is the motivation for the force network ensemble (FNE), which samples all valid force networks in the spring representation of a packing with equal probability.

The rigidity matrix, $\mathcal{R}$, represents a granular system as an unstressed spring network by encoding the normalized contact force vectors $\hat{n}_{ij}$ between pairs of particles i and j as

$$\mathcal{R}^{k\gamma}_{\langle ij \rangle} = \left(\delta^k_j - \delta^k_i\right) \hat{n}^\gamma_{ij}, \tag{3.1}$$

where k indexes particles, γ indexes spatial dimensions, and δ is the Kronecker delta [12, 23–25]. In periodic boundary conditions the minimum number of contacts required for stability for N particles in dimension d is [27]

$$N_c^* = Nd - d + 1, \tag{3.2}$$

and a system with exactly N_c^* contacts will have one stable force network configuration. For each additional contact in excess of N_c^* the associated unstressed spring network will have an additional linearly independent mechanically stable force network. These linearly independent force networks are referred to as the "states of self stress" or SSS of the system. These can be easily computed as they are the left singular vectors of $\mathcal{R}$ associated with the zero singular values of $\mathcal{R}$, i.e. the vectors F_i such that $F_i\mathcal{R} = \vec{0}$. While these SSS in general contain compressional as well as tensional forces, physical packings of frictionless spheres are constrained to compressional

forces. Thus we consider the FNE to be the set of linear combinations of the SSS which are positive semidefinite.

In previous work, we demonstrated that by considering the geometric nature of the SSS of a system, one can calculate the volume of the positive semidefinite linear combinations and from that the entropy of the force networks [12]. Further contemplation of this geometry has led us to examine the boundaries of this volume, which correspond to sets of contacts which are extraneous to the mechanical stability of the system. In particular, we focus on systems with exactly 2 states of self stress (2SSS), which are thus geometrically confined to have exactly two such boundaries. Each boundary corresponds to a set of contacts (typically each containing exactly one contact) which are unnecessary for mechanical stability of the packing. The breaking of this unnecessary contact results in a packing with just a single SSS (1SSS). In this work, we show that (i) between rearrangements, the force network ensemble of a system is stable under decompression, and (ii) that these boundaries of the volume of allowed force space identify the contacts that may be broken under decompression.

Computational Methods

We use pyCudaPacking [21], a GPU-based simulation engine, to generate monodispersed three dimensional harmonic soft sphere packings in periodic boundary conditions. We minimize the packings using the FIRE minimization algorithm [22] using quad precision floating point numbers in order to achieve sufficient resolution on the contact network near the jamming point. Using the same methods as in Refs. [14, 48], we start with randomly distributed initial positions at a packing fraction φ far above jamming and apply a search algorithm to create systems approximately logarithmically spaced in excess packing fraction, $\Delta\varphi$. We generate systems finely spaced in $\Delta\varphi$ (100 steps/decade) so that we may probe the dynamics of the transition from 2SSS to 1SSS. We continue this process until the system has exactly one state of self stress. We generate datasets of 500 systems at $N = 128, 1024$ and 100 systems at $N = 8192$. We measure the pressure P from the trace of the stress tensor as in Ref. [5] and denote the pressure at which the system transitions from 2SSS to 1SSS as P^*.

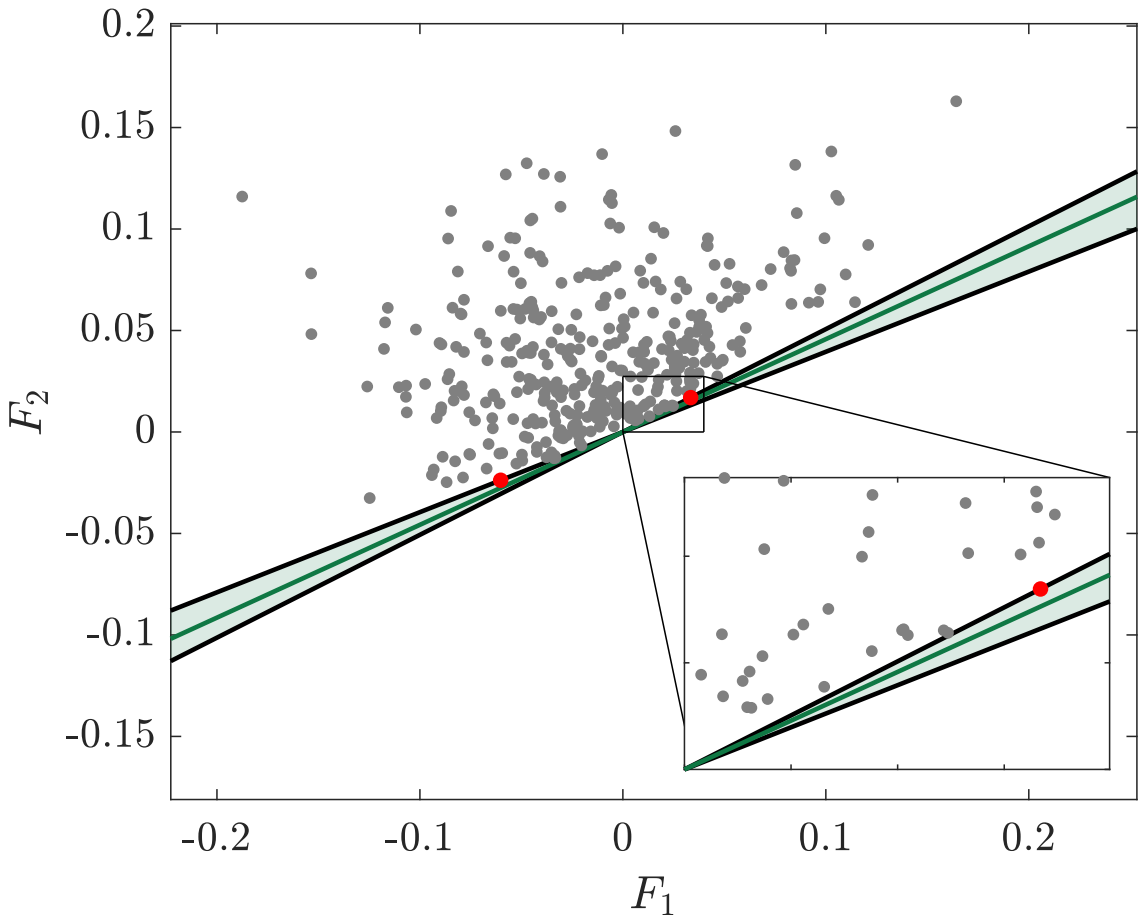

FIGURE 6. Scatter plot of the loads on each contact in the two states of self stress F_1 and F_2 for a typical system ($N = 128$) at 2SSS. Black lines represent the two linear combinations of force eigenvectors at the boundary of the allowed region of force space, shaded green. The two contacts which define these boundaries are shown in red. Green line shows linear combination that reconstructs the measured physical forces. Inset shows a region near the origin in greater detail. For a more pedagogical explanation see figure 1 in [12].

Results

The force network ensemble is the set of linear combinations of these SSS for which all forces are positive semi-definite. This defines a region in force space, the boundaries of which are the linear combinations of the SSS that bring the load on a contact or set of contacts to zero. In a system with 2SSS, one can exploit the orthogonality of the SSS to choose the linear combination that yields zero force on any given contact. The imposition of this constraint necessarily reduces the number of SSS by one, and within the context of the force network ensemble is equivalent to breaking a contact. However, with most contacts, this will result in negative forces (i.e. tensile

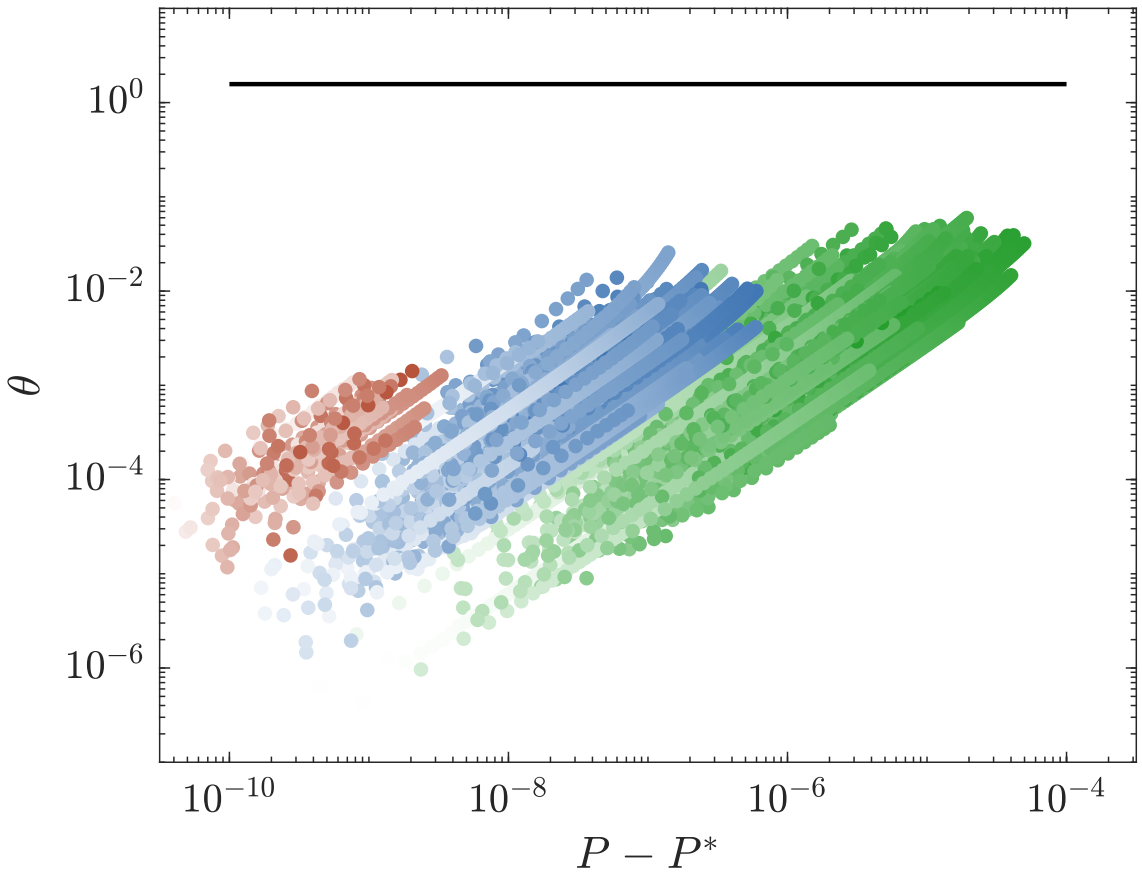

FIGURE 7. Angle θ between the force spaces of a system at a pressure P and P^*. Perpendicular force spaces would have $\theta = \pi/2$, shown as a black line. Data shown for N=128 (green), 1024 (blue), and 8192 (red), with opacity proportional to P.

loads) on some of the contacts unless the contact chosen is on the boundary of the allowed volume of force space. We demonstrate this geometrically in figure 6.

As a system decompresses, the geometry of the contact network changes. This is reflected in the rigidity matrix and thus results in changes in the null space of the loads. Since our systems are at 2SSS, this null space is always a two-dimensional plane within the N_c dimensional space of allowed loads on bonds. We characterize how this plane evolves by computing its angle θ relative to its final configuration at $P = P^*$. We define the angle θ between 2SSS force spaces $\mathcal{F}$ and $\mathcal{G}$ (with basis vectors $\hat{F}_i$ and $\hat{G}_i$) as [49]:

$$\cos(\theta) = \frac{|\wedge^2 g(\mathcal{F},\mathcal{G})|}{\sqrt{\wedge^2 g(\mathcal{F},\mathcal{F}) \wedge^2 g(\mathcal{G},\mathcal{G})}} \tag{3.3}$$

where

$$(\wedge^2 g)(\mathcal{F},\mathcal{G}) = \det \begin{pmatrix} \hat{F}_1 \cdot \hat{G}_1 & \hat{F}_1 \cdot \hat{G}_2 \\ \hat{F}_2 \cdot \hat{G}_1 & \hat{F}_2 \cdot \hat{G}_2 \end{pmatrix}. \tag{3.4}$$

While uncorrelated 2 dimensional planes drawn through the N_c dimensional force space are nearly perpendicular (i.e. $\theta \sim \frac{\pi}{2}$), we show in figure 7 that the force space volumes of our systems are always nearly aligned, even over wide ranges of pressure. This shows that the force network ensemble of a packing is stable under decompression, at least between rearrangements. Thus, it should be possible to use the force network ensemble to predict the evolution of the physical forces as the pressure is varied.

In a system at 2SSS, the space of normalized linear combinations of the SSS is a one dimensional space of rotations, as any stable force configuration f can be described by a mixing angle α such that $f = \sin(\alpha)F_1 + \cos(\alpha)F_2$, where F_1 and F_2 are the linearly independent SSS. While the physical forces in the packing are instead calculated from the overlaps, they represent a stable force network and as such we are always able to express them with a mixing angle in this way, up to machine precision and an overall scale factor. In the intervals between contact changes, we may thus consider the physical forces in the packing as flowing within this space of SSS, which is only gently changing as shown in figure 7. In figure 8(a), we show the mixing angles that describe the position within this space for the physical forces of a 2SSS system as it decompresses towards $P = P^*$. By following these mixing angles as a system decompresses, we see how the physical forces in the system approach and reach one of the 1SSS states on the boundaries of the 2SSS space. As an example, we can follow the upper red curve in figure 8(a) down in pressure towards the contact break, and we see that this system has a kink around $(P - P^*)/P^* \sim 1.3$. This arises from the exchange of the contact that originally formed the boundary of the allowed force space for another, which can be seen graphically in figure 8(b). Thus a prediction made with the boundary contact above that pressure will fail. The interchange in this manner of boundary contacts with other contacts that were intitially near the boundary is relatively unusual and is the sole failure mode of our prediction.

In a 2SSS system, there are always exactly two boundaries on the edge of the force space which correspond to two sets of "breakable contacts." Each of these sets of contacts usually

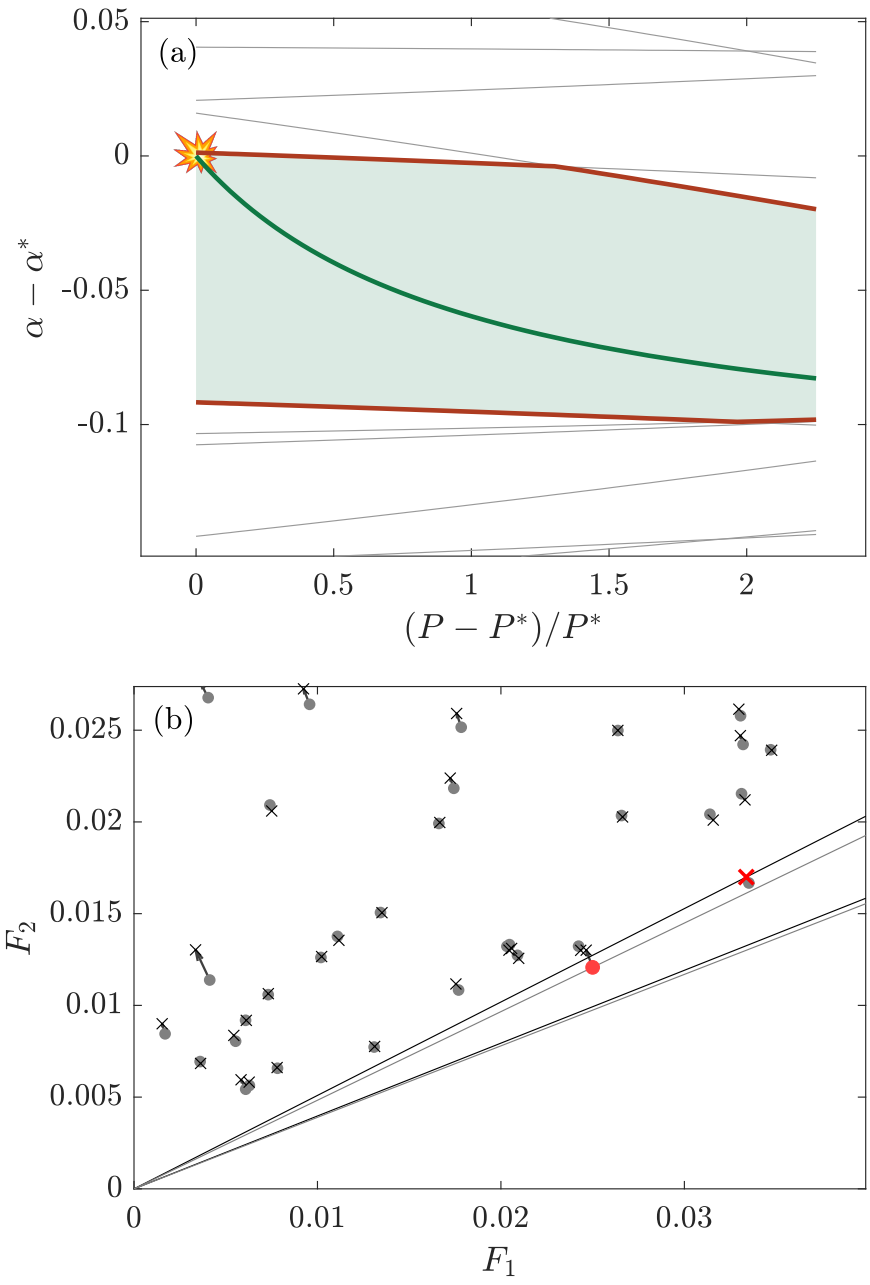

FIGURE 8. a) Evolution of mixing angle representation of the force space under decompression for the system in figure 6 over the range of pressures for which the system is at 2SSS. Position in force space is shown as mixing angles $\alpha - \alpha^*$ where α^* is the mixing angle of the system at the contact breaking event. Green shaded region shows all mixing angles for positive-definite force networks. Green line shows the physical forces. Red lines show the positive semi-definite boundaries. Grey lines show mixing angles which would bring other contacts to zero force. b) Evolution of the system in force space, shown as in the inset to figure 6. The highest and lowest pressures at which the system is at 2SSS are shown as grey circles and black x's, with arrows between them. "Breakable contacts" on the edge of force space are shown in red.

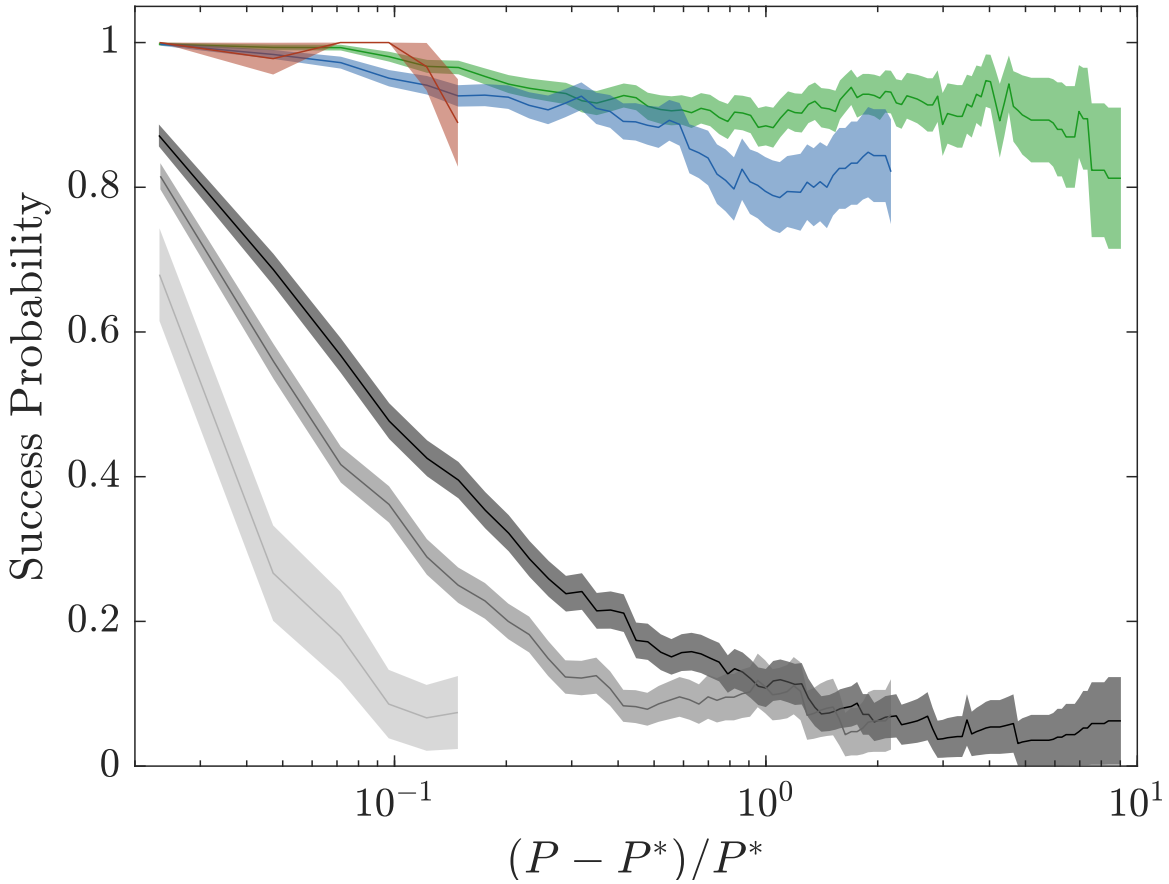

FIGURE 9. Probability of predicting contact breaking by FNE versus scaled pressure, for systems decompressing from 2SSS to 1SSS. As in fig. 7, N=128 (green), 1024 (blue), 8192 (red). Probability of smallest force in the system breaking is shown for $N = 128$ (dark grey), 1024 (medium grey), 8192 (light grey).

contains just one contact, but sometimes breaking a contact will form a rattler particle, all of whose contacts will thus be in the set of breakable contacts. In figure 9, we show the probability that one of these sets of "breakable contacts" is in fact broken under decompression from 2SSS to 1SSS. We find that the contacts predicted by the FNE are strongly predictive (greater than 80%) over the full range of pressures for which the system has 2SSS. This is in sharp contrast to the naïve prediction from affine response, that the smallest contact will break. Affine response is predictive very close to the contact breaking event, but falls to zero at higher pressures.

We examined the real space correlations between pairs of breakable contacts and found no correlation in position or angle subtended between contact vectors. However, we find that breakable contacts are more likely to occur between particles with higher than average contact

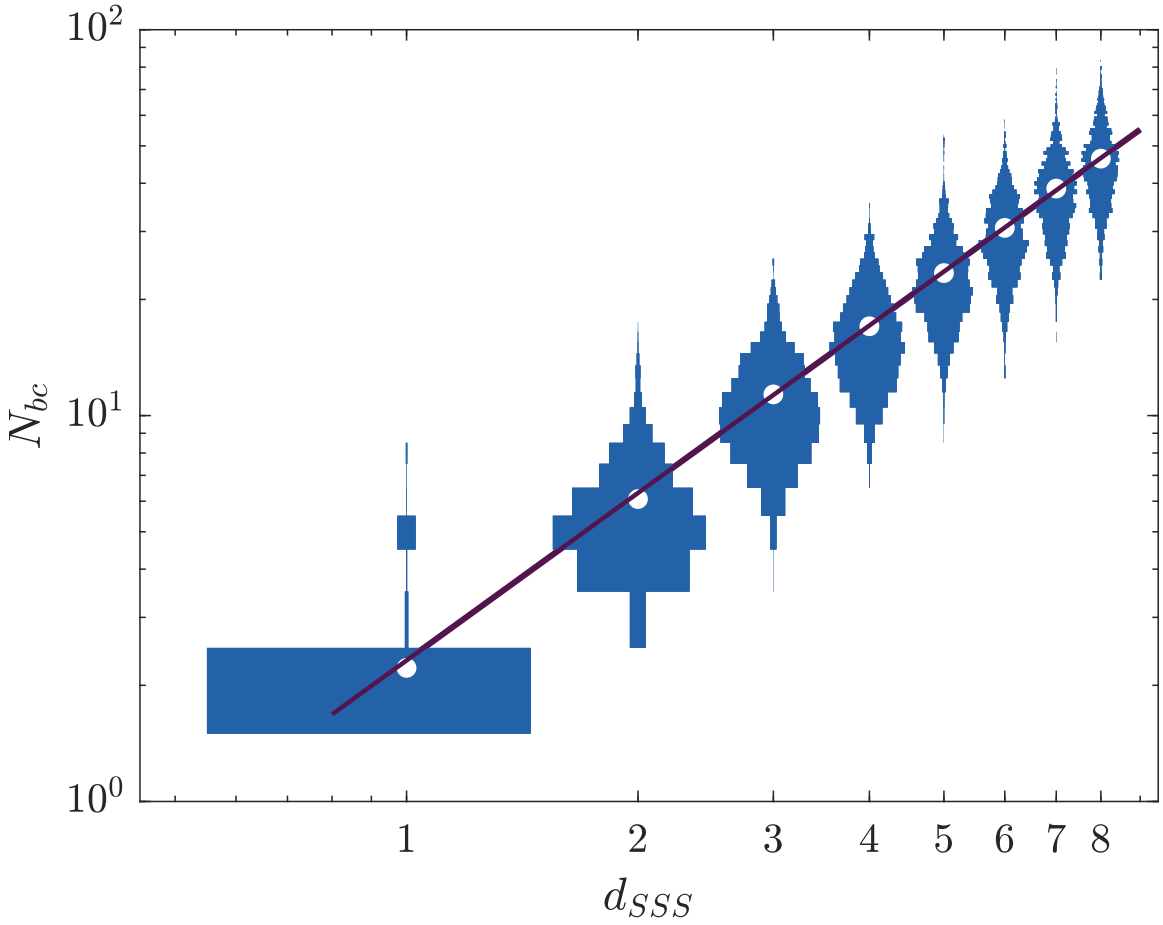

FIGURE 10. Histogram of the number of breakable contacts, N_{bc}, at each number of dimensions of the space of SSS, d_{SSS}, for $N = 128$. Purple line shows the empirical fit $N_{bc} \approx 2.43 d_{SSS}^{1.44}$.

number ($z \sim 6.4$). Such particles are thus more likely to have a contact that is unnecessary for system stability. This stands in contrast to the soft spot literature, in which particles with fewer contacts are identified as more likely to rearrange [35, 42–44]. This difference arises because soft spots exclusively identify instabilities, but the FNE also predicts the more numerous stable contact changes involving more highly coordinated particles.

At 2SSS, the two "breakable contacts" are excellent predictors of contact breaking events. At increased pressure, the number of contacts and thus SSS increase. In figure 10, we examine the relationship between the number of predicted breakable contacts, N_{bc} and the number of states of self stress, N_{SSS}. We examine the scaling of N_{bc} as a function of the dimensionality of the normalized SSS, $d_{SSS} = N_{SSS} - 1$. At 2SSS, the breakable contacts exist at the endpoints of a line which represents the space of allowed mixing angles. This typically results in two breakable

contacts, one at each endpoint, but may instead result in $N_{bc} \geq 5$ by creating a rattler at one endpoint (i.e. four or more contacts lost at that endpoint). We rarely find $N_{bc} = 3, 4$ which can only arise from degeneracies or numerical instabilities in the 1SSS force network. At 3SSS, the boundaries of the allowed force space are the edges of a polygon, and at higher SSS the facets of a polytope. These polytopes must have at least d_{SSS} boundaries, but may have arbitrarily many and thus arbitrarily many breakable contacts. We characterize the distribution of number of breakable contacts at each SSS by their mean, and find the means to be well fit by a power-law.

We conjecture that even at higher than 2SSS, the FNE may be used to predict contact breaking events. It has recently been shown that 86% of contact breaking events are reversible network events rather than rearrangements [45, 46]. We would thus expect that these reversible contact breaking events are well described by the FNE, and as such one could use our methods to predict the possible final 1SSS systems from a system with several contacts over 2SSS, with a success probability that scales as $P \sim 0.86^{d_{SSS}}$. We note however that while the physical forces of our packings were found precisely in the force network ensemble, this may fail at significantly higher pressures, because the force network ensemble is calculated from the unstressed spring network representation of a packing, whereas there exists a prestress on the physical forces.

Conclusions

We have shown that the force network ensemble of jammed systems remains approximately static between contact change events, and as such may be used to identify defective contacts. We have further shown that for 2SSS systems, these identified defective contacts are highly likely to break under decompression. While in spirit these defects can be thought of as analogous to soft spots, we emphasize two key differences here: (1) Soft spots identify locations of instabilities, while the force network ensemble identifies locations of both instabilities and stable contact network changes, and (2) While soft spots may be identified using just local information, the FNE approach by definition invokes global information. One might wish to use local information to find these defects, and there exists local structure to the force networks when the system is far from jamming [50]. However, at the jamming point the system becomes marginal, and as such any change in the contact network impacts the whole force network. For this reason we believe

that it would not be possible to identify these defective contacts near jamming without global information.

By restricting our study to 2SSS systems under decompression, we have explored only a limiting case of the space of the force network ensemble. We hope however that this serves as a gateway for future work, especially in exploring the force network landscape for systems with a greater number of SSS, where many more defects are predicted. One could also apply a modified version of these methods to identify force network defects in systems under shear. Our protocol identifies both stable contact changes and those that lead to instabilities. One further interesting remaining question is whether these can be differentiated from each other via the force network ensemble, giving a more complete picture of the defects within the system.

CHAPTER IV

MEAN-FIELD PREDICTIONS OF SCALING PREFACTORS MATCH LOW-DIMENSIONAL JAMMED PACKINGS

Introduction

Granular materials exhibit universal properties regardless of the material properties of the individual grains [21, 51, 52]. The jamming transition is a critical point near which properties such as pressure, packing fraction, or number of excess contacts, among others, scale as power laws. Scaling theory summarizes and condenses these power law relationships, but no first-principles theory of jammed systems at finite dimensions exists. The replica mean-field theory of glasses and jamming has been shown to be exact in the infinite dimensional limit [53, 54]. To do so it relies on the assumption that there are no correlations between neighbors, fundamentally at odds with low-dimensional systems. As such, mean-field predictions should not be expected to hold in low dimensional-jamming, and some results, most notably the packing fraction at jamming, deviate from the mean-field predictions [21, 55]. However, despite the fact that low dimensional systems have highly correlated neighbors the scaling relations are precisely the same as those found in infinite dimensions [5, 6, 56]. Many other results predicted by the mean field have also been observed in low dimensional jamming, suggesting that they may be provable without the mean field approximation [21, 52, 57–60].

Here, we move one step further in the comparison between low-dimensional jamming and mean-field jamming by probing not only scaling relations but also prefactors between a handful of properties: pressure P, excess contacts δz, and excess packing fraction above jamming $\Delta\varphi$. We demonstrate the continued success of the mean field in describing low-dimensional systems by quantitatively verifying the mean-field predictions for these prefactors. Thus, the mean-field approximation is overzealous: one need not have vanishing correlations in order to obtain these results. In this spirit we provide a first-principles proof of the relation between pressure and excess packing fraction free of the mean-field assumptions. These results call out for proofs for all of the other universal relations of the jamming transition.

Background

Granular materials undergo a jamming transition at a critical packing fraction φ_j. The number of force bearing contacts between grains jumps abruptly from zero to the minimum number sufficient to support global rigidity and thus global pressure, Z_c. In a packing of N frictionless, spherical particles in d dimensions, $Z_c = Nd + 1 - d$ [27, 51].

We limit our study to spherical particles interacting through a harmonic contact potential given by

$$U_{ij} = \varepsilon \left(1 - \frac{|\mathbf{r}_{ij}|}{\sigma_{ij}}\right)^2 \Theta\left(1 - \frac{|\mathbf{r}_{ij}|}{\sigma_{ij}}\right), \tag{4.1}$$

where ε is the energy scale, $\mathbf{r_{ij}}$ is the contact vector between particles i and j, σ_{ij} is the sum of the radii of particles i and j, and Θ is the Heaviside step function. Thus, the total energy $U = \frac{1}{2}\sum_{ij} U_{ij}$. From this potential, the forces between particles can be calculated as

$$\mathbf{f}_{ij} = \frac{2\varepsilon}{\sigma_{ij}} \left(1 - \frac{|\mathbf{r_{ij}}|}{\sigma_{ij}}\right) \Theta\left(1 - \frac{|\mathbf{r_{ij}}|}{\sigma_{ij}}\right) \hat{r}_{ij}. \tag{4.2}$$

We compute a unit and dimension independent pressure using the microscopic formula [5, 61]

$$P \equiv -\frac{\bar{V}_p}{\varepsilon}\frac{dU}{dV} = \frac{\bar{V}_p}{\varepsilon V d}\sum_{i,j} \mathbf{f}_{ij} \cdot \mathbf{r}_{ij}, \tag{4.3}$$

where V is the volume of the system and $\bar{V}_p$ is the average particle volume.

For soft spheres the packing fraction φ can be increased, leading to new contacts and an increased pressure. We thus consider three natural quantities that measure distance from jamming:

- excess packing fraction, $\Delta\varphi = \varphi - \varphi_j$
- excess contacts per particle, $\delta z = (Z - Z_c)/N$ where Z is the number of contacts
- pressure P

The relationships between these quantities are predicted by mean-field theory as [54]:

$$P = C_{p\varphi}\Delta\varphi \tag{4.4}$$

$$\delta z = C_{zp} P^{1/2} \tag{4.5}$$

with prefactors $C_{p\varphi}$ and C_{zp} which are functions only of spatial dimension [5]. These and other scaling relationships have been previously explained by approximate theories [62–65] and computationally confirmed in low-dimensional jamming [5, 27, 51, 56]. They are summarized concisely by the scaling theory of the jamming transition [6]. The scaling exponents in $d \geq 2$ match those in mean field, suggesting that the transition behaves like a critical point with upper critical dimension $d_u = 2$. Moreover, mean-field theory predictions of these prefactors can be derived as [54, 66]:

$$C_{p\varphi} = \frac{1}{d}\hat{C}_{p\varphi} \tag{4.6}$$

$$C_{zp} = \frac{d}{\sqrt{2^d}}\hat{C}_{zp} \tag{4.7}$$

where $\hat{C}_{p\varphi}$ and $\hat{C}_{zp}$ are finite constants in the $d \to \infty$ limit, which have not yet been explicitly calculated. Note that these relations are presented in a particular choice of units in the literature. We include details of the conversion to our dimensionless units in the Supplemental Material. *A priori*, it is not expected that these predictions will apply in low dimensions, in which the mean-field assumption is not warranted. Even above upper critical dimensions, mean-field theories are not generally expected to correctly compute prefactors, or even the purportedly universal amplitude ratios. Beyond scaling exponents, to our knowledge, the critical cluster shape in percolation and related phenomena [67, 68] and the Binder cumulant in the Ising model [69–71] are the only quantities which are known to be equal to their mean-field values above the upper critical dimension. Even though these prefactors for jamming scaling relationships have been measured and reported [5, 12], because they are not expected to be equal to their mean-field values they have not received substantial theoretical attention. An approximate calculation of the related prefactor between the shear modulus and number of excess contacts has been performed in three dimensions [64].

Computational methods

We use pyCudaPacking [21], a GPU-based simulation engine, to generate energy minimized soft (or penetrable) sphere packings. We do so for number of particles $N = 8192 - 32768$ and dimension $d = 2 - 10$. Our results suggest that $N = 8192$ is large enough to avoid finite size

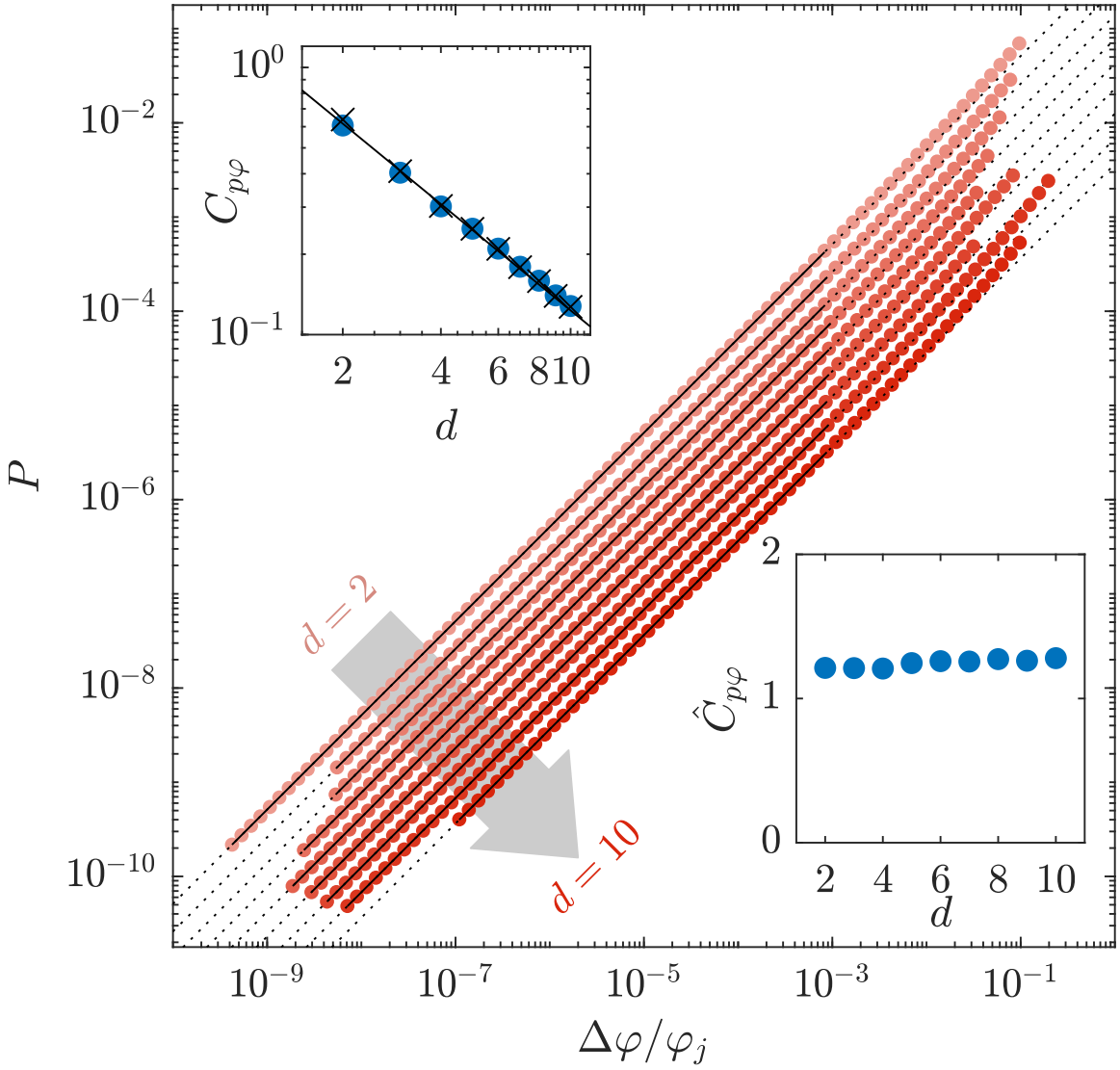

FIGURE 11. Measured pressure scales linearly with scaled excess packing fraction for systems from $d = 2$ to $d = 10$. Measured values for φ_j in our protocol are included in the Supplemental Material. Black lines show fits for $C_{p\varphi}$ using Eq. 4.4. We exclude from the fit data with $\Delta\varphi/\varphi_j > 10^{-3}$, to avoid the effect of larger overlaps causing deviations from this power law. Dotted lines show the extension of fits beyond fitted range. Upper inset shows the measured values of $C_{p\varphi}$ (blue circles) to scale in agreement with the mean-field prediction Eq. 4.6, shown as a fit to a black line with $\hat{C}_{p\varphi} \approx 1.23$. Moreover, they are in precise agreement with predicted values from Eq. 4.15 (marked with black $\times$'s). Lower inset shows measured values of $\hat{C}_{p\varphi}$ calculated from the measured values of $C_{p\varphi}$ and eqn 4.6. While each prefactor is measured from a single system, the prefactors for a second, identically constructed dataset were calculated to be well within the bounds of the marker size.

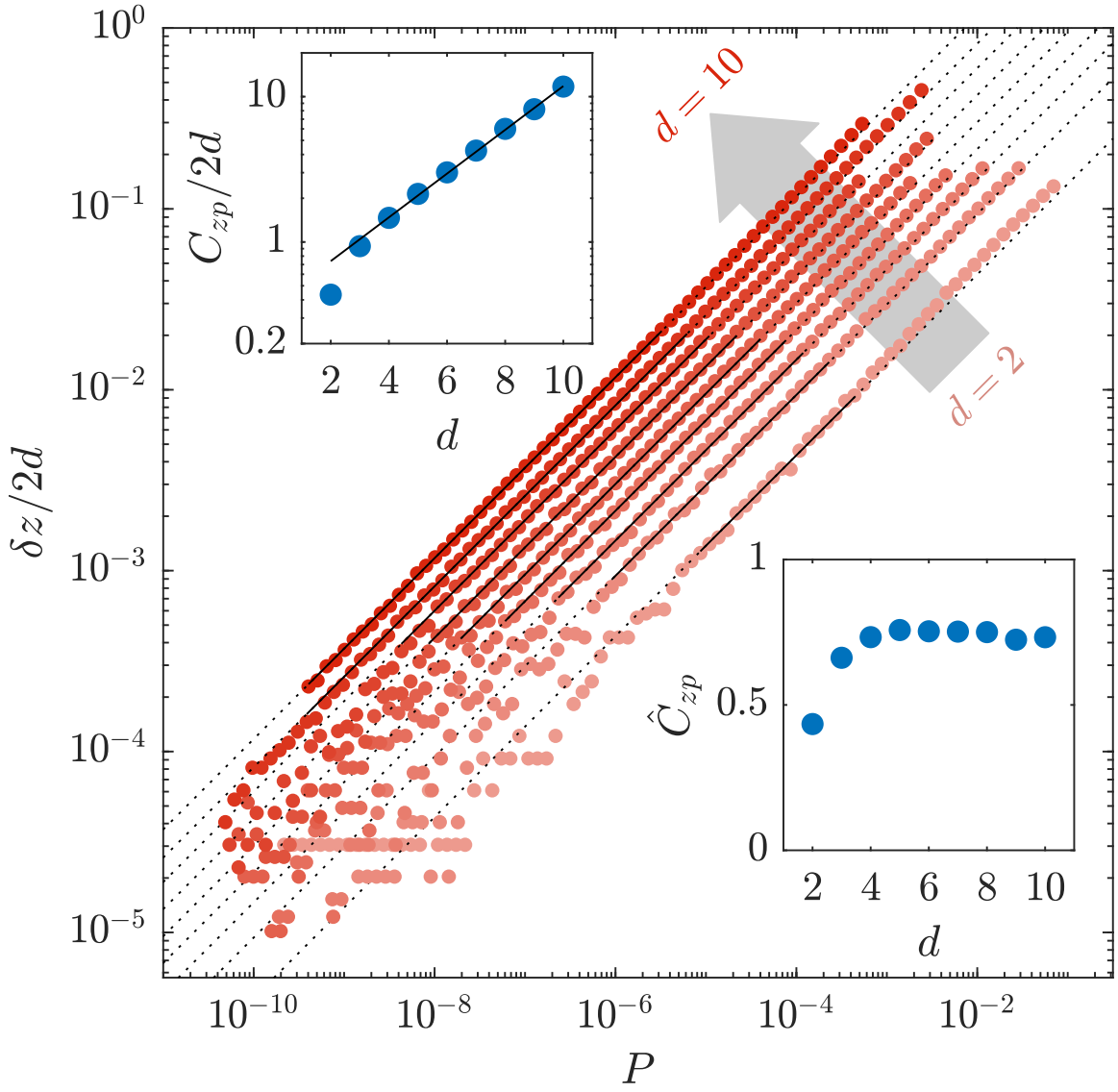

FIGURE 12. Measured excess contacts scales with the square root of pressure for systems from $d = 2$ to $d = 10$. Black lines show fits for C_{zp} using Eq. 4.5. For our fits, we ignore high pressure data as in Fig. 11, and additionally exclude data with less than 40 excess contacts to avoid fitting to small number fluctuations. Dotted lines show the extension of our fits beyond fitted range. Lower inset shows the measured values of C_{zp} (blue circles), which scale in agreement with the mean-field prediction Eq. 4.7, shown as a fit to a black line and with $\hat{C}_{zp} \approx 0.74$. Upper inset shows measured values of $\hat{C}_{zp}$ calculated from the measured values of C_{zp} and Eq. 4.7. While each prefactor is measured from a single system, the prefactors for a second, identically constructed dataset were calculated to be well within the bounds of the marker size.

effects in $d < 9$, which we have verified in $d = 8$ by comparing our packing at $N = 8192$ with one at $N = 16384$, finding no deviation. For $d = 9$ and $d = 10$ we use system sizes of 16384 and 32768, respectively. The particles are monodisperse, except in two dimensions in which we use equal numbers of bidisperse particles with a size ratio of 1:1.4 to prevent crystallization.

The packings are subject to periodic boundary conditions. We minimize the packings using the FIRE minimization algorithm [22] using quad precision floating point numbers in order to achieve resolution on the contact network near the jamming point.

Using the same methods as described in Ref. [23], we start with randomly distributed initial positions, and apply a search algorithm to create systems approximately logarithmically spaced in $\Delta\varphi$. At each step we use the known power law relationship between energy and $\Delta\varphi$ to calculate an estimate of φ_j. We use this estimate to approximate $\Delta\varphi$ and determine the next value of φ in an effort to logarithmically space $\Delta\varphi$ values. We then adjust the packing fraction to this value of φ by uniformly scaling particle radii and minimizing the system. We continue this process until the system is nearly critically jammed, i.e. has exactly one state of self stress. We then use the known power law relationship between pressure and $\Delta\varphi$ to fit the dataset and precisely calculate φ_j (with error less than the smallest value of $\Delta\varphi$) from which we calculate $\Delta\varphi$ at each value of φ.

Results

Figure 11 shows the measured linear scaling of pressure with packing fraction separately for each dimension. We fit the data to Eq. 4.4 to find $C_{p\varphi}$, considering only data close to jamming to avoid fitting to high pressure deviations from the scaling power law. The measured values of $C_{p\varphi}$ are shown in the inset to confirm the $1/d$ dimensional scaling predicted by mean-field theory in Eq. 4.6. A fit to this scaling provides a value of $\hat{C}_{p\varphi}$ of 1.23.

Figure 12 shows the measured square root scaling of excess contacts with pressure separately for each dimension. We fit the data to Eq. 4.5 to find C_{zp}, the values of which are shown in the inset. Beginning around three dimensions, the values of C_{zp} confirm the dimensional scaling predicted by mean-field theory in Eq. 4.7, and a fit to this scaling provides a value of $\hat{C}_{zp}$ of 0.74.

The values of both $C_{p\varphi}$ and C_{zp} are roughly consistent with values measured in previous studies [5, 12]. It has been recently suggested that the prestress, i.e., the normalized ratio of the first and second derivatives of the potential as defined in Ref. [72], is a better candidate to dedimensionalize the relationship between pressure and excess contacts. However, we find a substantially better collapse of our expected form of pressure than with prestress. For more details on prestress, see the attached Supplemental Material.

Discussion

The close agreement of our data with the mean-field predictions in low dimensions suggests that the mean-field assumption is not essential to derive these scaling and prefactor relations. In the spirit of discovering proofs for these relations free of the mean-field assumption, we expand on an earlier calculation of the bulk modulus scaling [63] to show that such a calculation can also explain the scaling of $C_{p\varphi}$ with spatial dimension and the precise value of $\hat{C}_{p\varphi}$.

From taking a derivative of Eq. 4.4, we see immediately that $C_{p\varphi}$ may be expressed in terms of the bulk modulus, $K \equiv V\frac{d^2U}{dV^2}$, at jamming:

$$C_{p\varphi} = \frac{\bar{V}_{\mathrm{p}}V}{\varphi\varepsilon}\frac{d^2U}{dV^2} = \frac{V}{N\varepsilon}K. \tag{4.8}$$

We note that this approximation slightly overestimates $C_{p\varphi}$: the apparently linear average stress-strain curves of jammed packings are actually the average of many piecewise linear curves with discontinuous drops in stress, thus the average slope is slightly less than the instantaneous slope [73].

At the unjamming point, the linear response of the system is that of a network of unstretched springs. Thus, at lowest order in pressure the bulk modulus is that of an unstressed spring network, which may be calculated in terms of the "states of self stress," vectors of possible spring tensions, $s \in \mathbb{R}^Z$, which do not produce any net force on a particle [63, 74, 75]. Here we explain how to carry out this calculation for a monodisperse system in the unjamming limit; a correction for polydispersity is handled in the Supplemental Material.

We begin by defining the set of "affine bond extensions," a vector $E \in \mathbb{R}^Z$ giving the amount by which each bond vector would increase under a unit volumetric expansion of the system. In linear elasticity, this simply induces an expansion of each length by $1/d$, so,

$$E_\ell = \frac{1}{d} r_\ell, \tag{4.9}$$

where we emphasize that ℓ indexes the contacts in the system rather than the particles; r_ℓ is the distance between a particular pair of particles.

In the case that all springs have the same spring constant k (e.g., monodisperse packings), the bulk modulus may be written as the projection of these affine moduli onto the states of self stress [63, 74, 75]. At jamming, there is only one state of self stress, and so the bulk modulus may be computed exactly using the projection onto only this one state of self stress [63],

$$K = \frac{k}{V} \left(\sum_{\ell=1}^{Z} s_{1,\ell} E_\ell \right)^2 \tag{4.10}$$

$$= \frac{2N\varepsilon}{dV} \frac{\langle f \rangle^2}{\langle f^2 \rangle} \tag{4.11}$$

In the near jamming limit, this one special state of self stress exists all the way down to the jamming point and can be expressed in terms of the vector of physical force magnitudes, f. For the packing to be in equilibrium, this set of contact forces must produce no net force on every particle, and thus by definition the vector f is always a state of self stress. The projection defined above requires states of self stress to be normalized, and so the state of self stress may be expressed as:

$$s_{1,\ell} = \frac{1}{\sqrt{\sum_l f_l}} f_\ell = \frac{1}{\sqrt{Z \langle f^2 \rangle}} f_\ell. \tag{4.12}$$

Furthermore at lowest order in P we have $r = \sigma$, and we assume $Z \approx dN$. Thus, Eq. 4.10 reduces to

$$K = \frac{Nk\sigma^2}{dV} \frac{\langle f \rangle^2}{\langle f^2 \rangle} = \frac{2N\varepsilon}{dV} \frac{\langle f \rangle^2}{\langle f^2 \rangle} \tag{4.13}$$

and thus via Eq. 4.8

$$C_{p\varphi} = \frac{2}{d} \frac{\langle f \rangle^2}{\langle f^2 \rangle}, \tag{4.14}$$

for monodisperse spheres. The full calculation in the Supplemental Material shows that in the polydisperse case this becomes

$$C_{p\varphi} = \frac{2}{d}\frac{\langle \sigma f \rangle^2}{\langle \sigma^2 f^2 \rangle}. \tag{4.15}$$

We find that the distribution of contact forces does not depend strongly on dimension, which we demonstrate and discuss in the Supplementary Material, including Refs. [23, 76]. We thus predict the scaling of $C_{p\varphi}$ to agree with the asymptotic mean-field scaling. Because this proof does not invoke the mean-field assumption, we expect this scaling to be correct in all dimensions. Moreover, we are able to calculate each value of $C_{p\varphi}$ by measuring the ratio of force distribution moments. These values are calculated as in Eq. 4.15, and are shown in Fig. 11 to precisely predict the values of $C_{p\varphi}$.

Conclusion

The mean-field theory of jamming predicts both the scaling exponents and the dimensional scaling of their prefactors. While the exponents have been previously verified, we have demonstrated that even some prefactors are well predicted in low dimensions by mean-field theory. Although these prefactors should be considered especially sensitive to finite dimensional corrections, we find the mean field prediction to be exact in low dimensions. Is this a generic phenomenon, or are the quantities we have chosen to study in this work somehow specially unaffected by finite dimensional correlations? Experience with critical phenomena suggests that although certain ratios of these prefactors (i.e. amplitude ratios) may be universal, the prefactors themselves should be both nonuniversal and challenging to compute, which has led to them being neglected. Our results demonstrate however that these prefactors may be computed exactly. These results call out for other theories of jamming and the glass transition which reproduce the mean-field results without such assumptions, or perhaps for a deeper understanding of why certain mean-field computations may be exact in finite dimensions. Additionally, our results suggest that in traditional critical phenomena mean-field theory may compute more for $d \geq d_u$ than has been previously appreciated.

Supplementary Material of "Mean-field predictions of scaling prefactors match low-dimensional jammed packings"

Measured values of φ_j

In Table 1 we show our measued values of φ_j. these values are used in calculating $\Delta\varphi$.

TABLE 1. Measured values of φ_j in dimensions 2-10.

d	2	3	4	5	6	7	8	9	10
φ_j	0.85	0.65	0.46	0.31	0.20	0.13	0.078	0.049	0.029

Mean Field Prediction of Pressure vs Packing Fraction

Mean field theory predicts that pressure scales with packing fraction as follows [54]:

$$\hat{P} = \hat{C}(\hat{\varphi} - \hat{\varphi}_j) \tag{4.16}$$

where $\hat{C}_{p\varphi}$ is a constant, and the hats over P and $\Delta\varphi$ signify that the quantities are scaled such to be fixed in the infinite dimensional limit, as follows:

$$\hat{P} = \frac{P^*}{\rho d} \tag{4.17}$$

$$\hat{\varphi} = \frac{2^d}{d}\varphi \tag{4.18}$$

where ρ is the number density, $\frac{N}{V}$, and P^* is the pressure which is calculated with assumed unit particle diameter. This relates to our pressure, P, as follows:

$$P = \frac{\varphi}{\rho}\frac{1}{d^2}P^*, \tag{4.19}$$

where the factor of $\frac{\varphi}{\rho}$ unwraps their assumption of unit particle diameter, and the factor of $\frac{1}{d^2}$ comes from their potential, which explicitly contains a dimensional term:

$$U^*(r) = \frac{\epsilon d^2}{2}\left(\frac{r}{\ell} - 1\right)^2 \Theta\left(\ell - r\right). \tag{4.20}$$

We can thus rewrite equation 4.17 in terms of our pressure P:

$$\hat{P} = \frac{d}{\varphi} P, \tag{4.21}$$

and therefore equation 4.16:

$$\frac{d}{\varphi} P = \hat{C} \frac{2^d}{d} (\varphi - \varphi_j) \tag{4.22}$$

$$P = \frac{\varphi}{d} \hat{C} \frac{2^d}{d} \Delta\varphi \tag{4.23}$$

$$P = \frac{1}{d} \hat{C} \hat{\varphi}_j (\Delta\varphi) \tag{4.24}$$

$$P = \frac{1}{d} \hat{C}_{p\varphi} (\Delta\varphi). \tag{4.25}$$

Where, noting that $\hat{\varphi}_j$ and $\hat{C}$ are constants in the infinite dimensional limit, we combine them as $\hat{C}_{p\varphi}$. Thus mean field predicts a simple $1/d$ scaling of the prefactor between pressure and excess packing fraction.

Mean Field Prediction of Pressure vs Number Of Excess Contacts

The number of contacts, z, is predicted by mean field theory to have the form [54]:

$$\frac{z}{2d} = 1 + \hat{C}_{z\varphi} \sqrt{\hat{\varphi} - \hat{\varphi_j}} \tag{4.26}$$

$$\frac{z}{2d} = 1 + \hat{C}_{z\varphi} \sqrt{\frac{2^d}{d}} \sqrt{\varphi - \varphi_j} \tag{4.27}$$

for some constant $\hat{C}_{z\varphi}$.

The number of excess contacts, δz, therefore is predicted to scale as follows:

$$\frac{\delta z}{2d} = \hat{C}_{z\varphi} \sqrt{\frac{2^d}{d}} \sqrt{\varphi - \varphi_j} \tag{4.28}$$

$$\delta z = 2d \hat{C}_{z\varphi} \sqrt{\frac{2^d}{d}} \sqrt{\varphi - \varphi_j}. \tag{4.29}$$

Mean Field Prediction of Packing Fraction vs Number of Excess Contacts

By combining equations 4.25 and 4.29, we can also predict the relation between δz and P:

$$\delta z = 2d\hat{C}_{z\varphi}\sqrt{\frac{2^d}{d}}\sqrt{\frac{d}{\hat{C}_{p\varphi}}P} \tag{4.30}$$

$$= 2d\hat{C}_{z\varphi}\sqrt{\frac{2^d}{\hat{C}_{p\varphi}}}\sqrt{P} \tag{4.31}$$

$$\tag{4.32}$$

where we define $\hat{C}_{zp} = \frac{2\hat{C}_{z\varphi}}{\sqrt{\hat{C}_{p\varphi}}}$.

Excess Contacts vs Excess Packing Fraction Prefactor Scaling

From eqns 4.4 and 4.5 we can simply relate δz and φ as follows:

$$\delta z = C_{z\varphi}\left(\Delta\varphi\right)^{1/2} \tag{4.33}$$

where clearly,

$$C_{z\varphi} = C_{zp}\sqrt{C_{p\varphi}}. \tag{4.34}$$

In figure 13, we show this scaling seperately for each dimension. We fit each line to eqn 4.33 to find the values of the prefactor $C_{z\varphi}$ in each dimension, the values of which are shown in the inset. These values agree well with both the mean field prediction above $3D$, shown as a black line, and our calculated value from C_{zp} and $C_{p\varphi}$, shown as black x's in figures 11 and 12.

Dimensional Dependence of Force Moment Ratios

In figure 14 we show that the ratio of force moments does not depend strongly on dimension. This empirical fact may seem at odds with previous reports of how the low-force part of the distribution differs from its mean-field form in low dimensions [23, 76]. The low-force part of the distribution has $P(f) \propto f^{\theta}$, where $\theta \approx 0.17$ in $d = 2$ smoothly rises to a $d = \infty$ value of $\theta \approx 0.42$. The high-force behaviour decays like an exponential or a stretched exponential; thus, we have computed the theoretical value of this moment ratio for distributions of the form

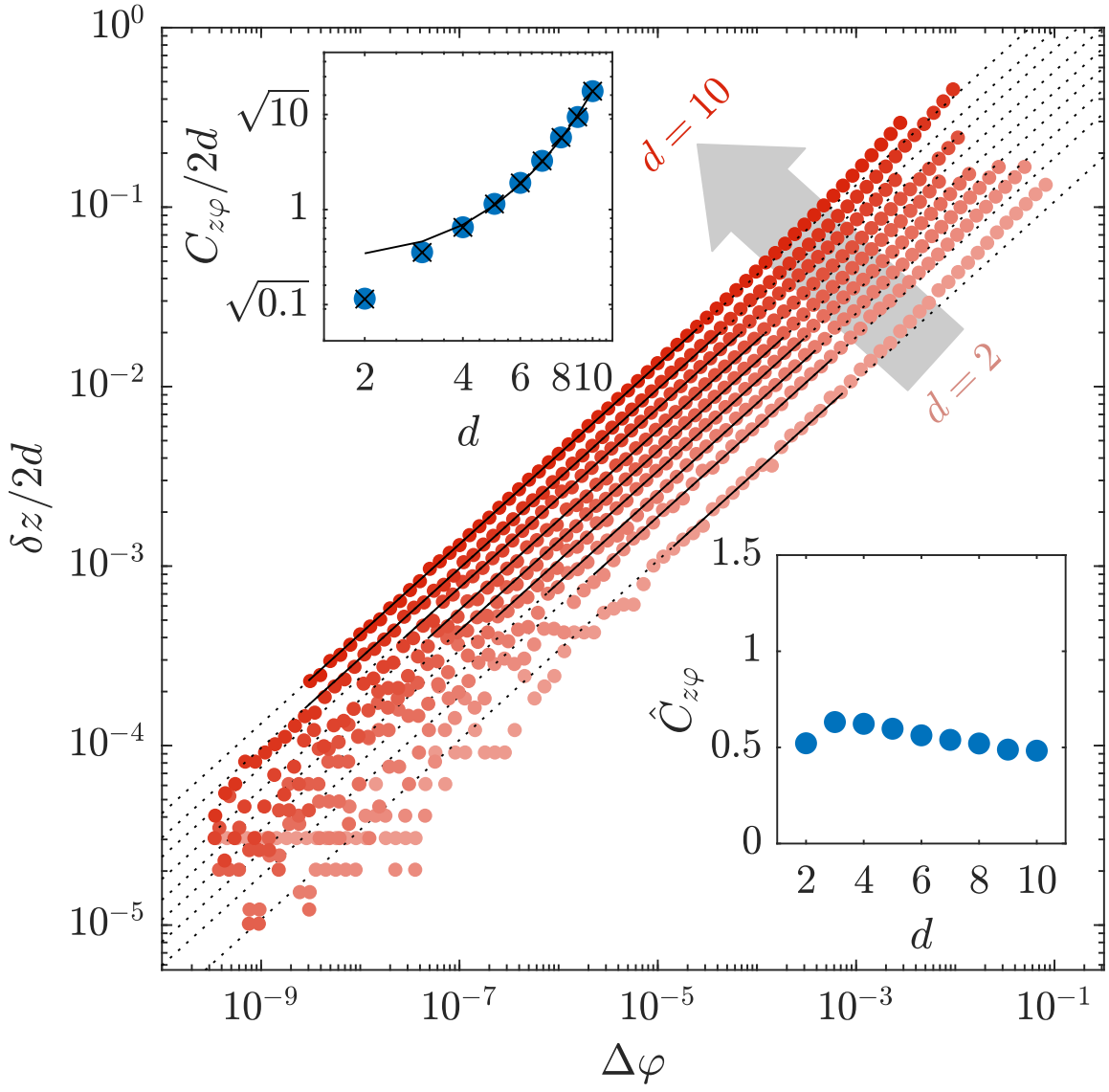

FIGURE 13. Measured excess contacts scales with the square root of excess packing fraction for systems from $d = 2$ to $d = 10$ (red circles). Black lines show the fits for C_{zp} using eqn 4.33. For our fits, we ignore data at high pressure and low contact number as in figure 12. Dotted lines show the extension of our fits beyond the fitted range. Inset shows the measured values of $C_{z\varphi}$ (blue circles), which scale in agreement with the mean field prediction eqn 4.29 using measured values of with $\hat{C}_{z\varphi} \approx 0.83$. Additionally, to note consistency we show that our measured values of $C_{z\varphi}$ agree well with values calculated from our measurements of $C_{p\varphi}$ and C_{zp} using eqn 4.34 (black x's).

$P(f) \sim f^{\theta} e^{-f/f_0}$ and $P(f) \sim f^{\theta} e^{-f^2/f_0^2}$, as shown in figure 15. We find that neither of these assumed distributions quantitatively predicts the measured moment ratio for the known values of θ, but they do show that the known variation in θ should not make us expect a large variation in this moment ratio.

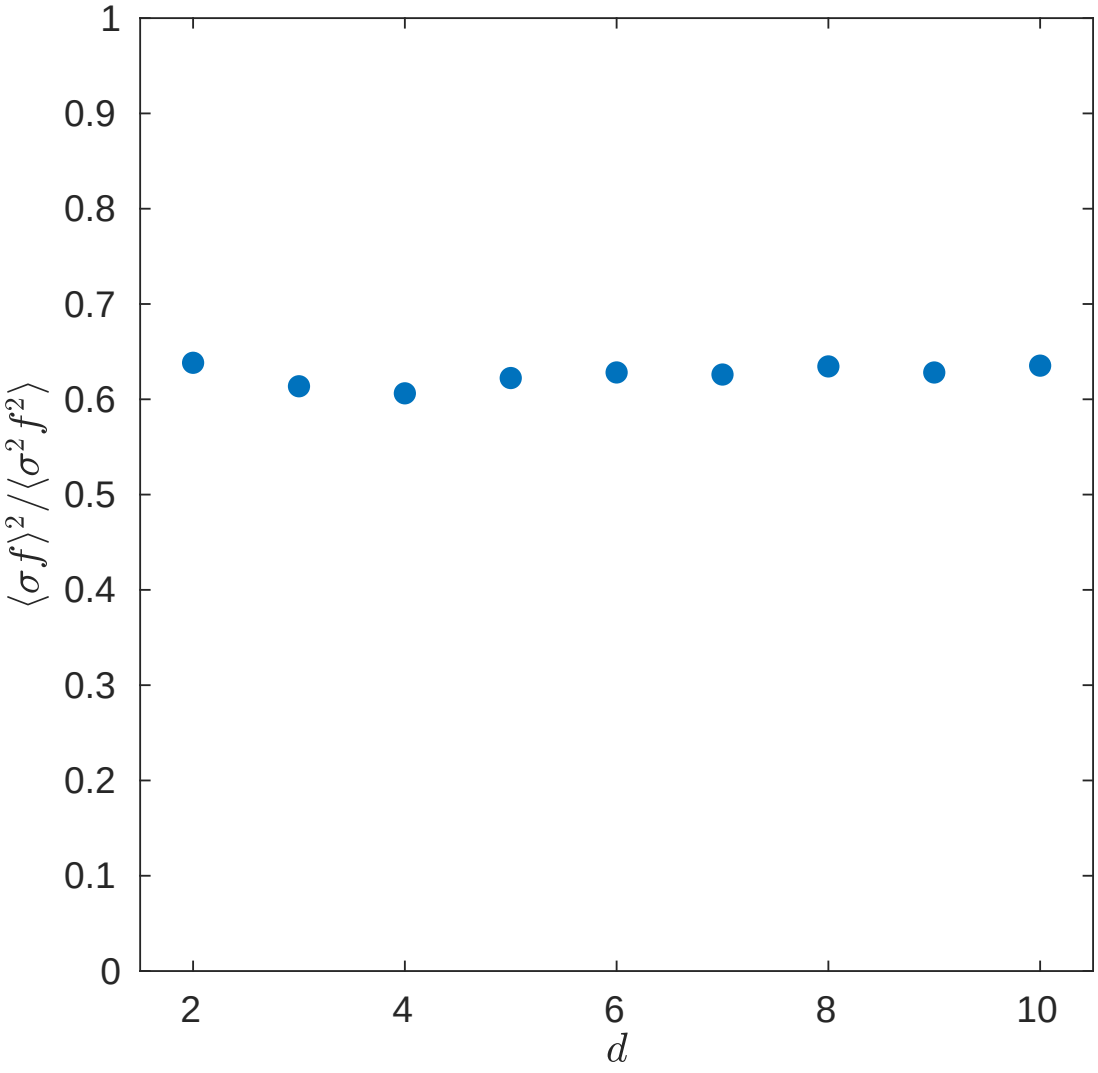

FIGURE 14. Dimensionless moment ratio of first and second moments of σf shows no dimensional dependence

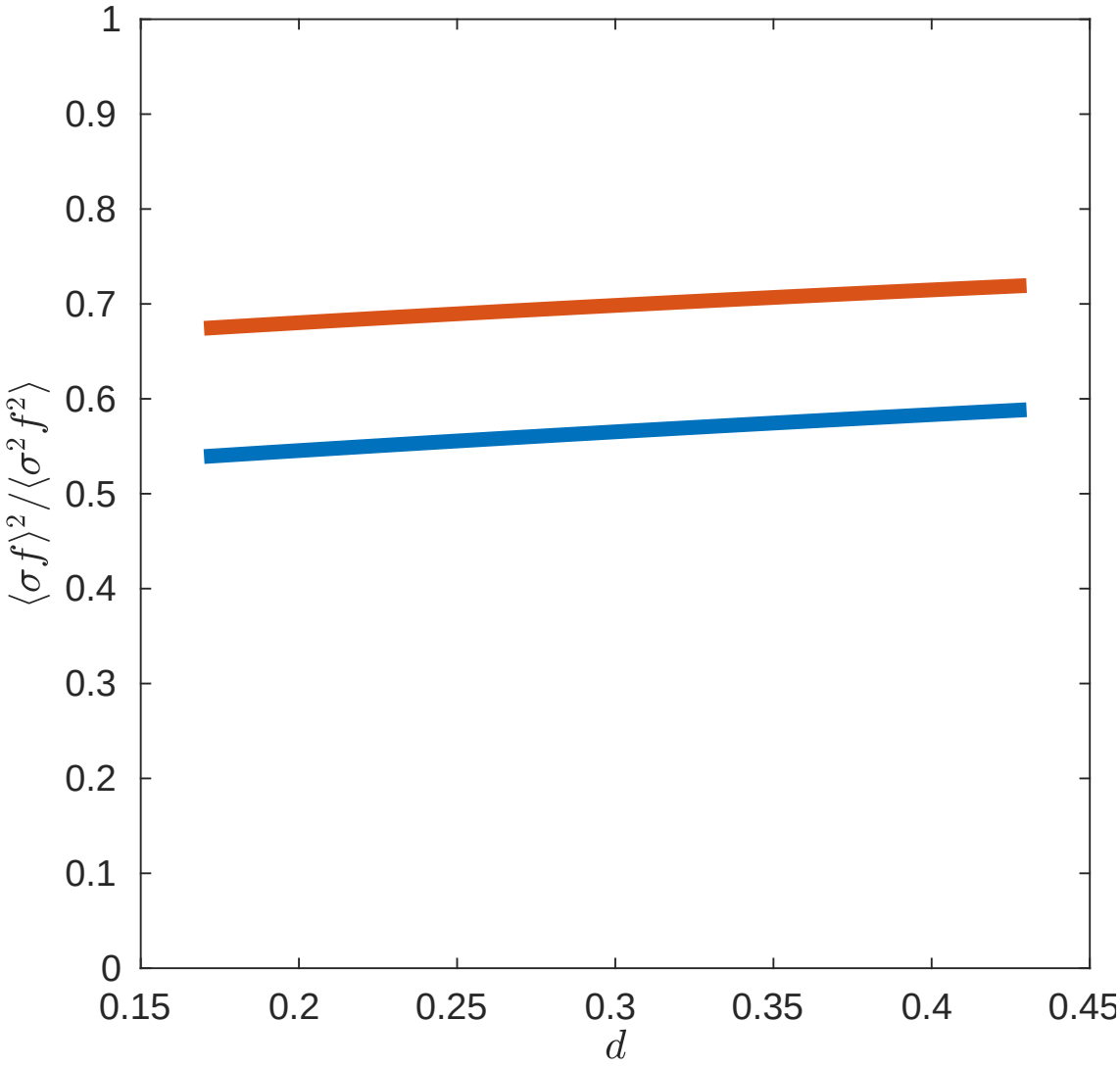

FIGURE 15. Neither the force distribution $f^\theta e^{-f/f_0}$ (blue) nor the distribution $f^\theta e^{-f^2/f_0^2}$ (red) predicts a strong θ dependence for the relevant moment ratio

Accounting for Polydispersity in Pressure vs. Packing Fraction Scaling

To account for the case with varying spring constants we also form the matrix of inverse spring constants

$$k^{-1} = \frac{1}{2\varepsilon} \begin{pmatrix} \sigma_{ij}^2 & & \\ & \ddots & \\ & & \sigma_{kl}^2 \end{pmatrix}. \tag{4.35}$$

and the projection operator onto the states of self stress

$$S = \sum_{i=1}^{N\Delta z} |s_i\rangle \langle s_i| . \tag{4.36}$$

In terms of these quantities, the bulk modulus may be written as [63, 74, 75]

$$\frac{\partial^2 E}{\partial V^2} = \frac{1}{V} \langle E| S \left(S \left(k^{-1} \right) S \right)^{-1} S |E\rangle . \tag{4.37}$$

In the one SSS approximation, we can evaluate the two projected quantities that we need to evaluate equation 4.37. Equations 4.9 and 4.12 give

$$S |E\rangle = \langle s_0|f\rangle |s_0\rangle = \frac{\langle r|f\rangle}{d\sqrt{\langle f|f\rangle}} |s_0\rangle = \sqrt{Z} \frac{\langle rf\rangle}{d\sqrt{\langle f^2\rangle}} |s_0\rangle , \tag{4.38}$$

and equations 4.35 and 4.12 give

$$Sk^{-1}S = |s_0\rangle \langle s_0|k^{-1}|s_0\rangle \langle s_0| = |s_0\rangle \frac{\langle \sigma^2 f^2\rangle}{2\epsilon\langle f^2\rangle} \langle s_0| \tag{4.39}$$

$$\left(Sk^{-1}S\right)^{-1} = |s_0\rangle \frac{2\epsilon\langle f^2\rangle}{\langle \sigma^2 f^2\rangle} \langle s_0| \tag{4.40}$$

Furthermore at lowest order in P we have $|r\rangle = |\sigma\rangle$, and we may assume $Z \approx dN$. Thus, equation 4.37 reduces to

$$K = \frac{2N\varepsilon}{dV} \frac{\langle \sigma f\rangle^2}{\langle \sigma^2 f^2\rangle}, \tag{4.41}$$

and thus via equation 4.8:

$$C_{p\varphi} = \frac{2}{d} \frac{\langle \sigma f\rangle^2}{\langle \sigma^2 f^2\rangle}. \tag{4.42}$$

Prestress Comparison

It has recently been suggested the relationship between prestress and number of excess contacts collapses perfectly when compared across dimensions [72]. We define prestress e as in ref. [72] as:

$$e = (d-1)\left\langle \frac{-V'(r_{ij})}{r_{ij}V''(r_{ij}}\right\rangle_{ij} \tag{4.43}$$

and expected to scale as:

$$\delta z = C_{ze}e^{\frac{1}{2}} \tag{4.44}$$

because it is proportional to pressure near the jamming transition [72]. In figures 17 and 16,, we examine the collapse of scaled excess contacts with prestress and compare it to the collapse of excess contacts scaled by the mean field prediction with pressure. In figure 17 we see that the collapse with prestress is not quite perfect - there is a clear upward trend. This stands in contrast to the inset of figure 16, which shows $\hat{C}_{zp}$ to be nearly constant above three dimensions.

In fact, close to jamming so that $r \approx \sigma$ and $Z \approx Nd$, our dimensionless pressure P as defined in equation 4.3 is related to the prestress by

$$P = \frac{\bar{V}_p}{\varepsilon V d}\sum_{i,j}\mathbf{f}_{ij}\cdot\mathbf{r}_{ij} \tag{4.45}$$

$$= \frac{\bar{V}_p}{\varepsilon V d}Z\langle f_{ij}r_{ij}\rangle_{ij} \tag{4.46}$$

$$= \frac{2\varphi Z}{d}\left\langle \frac{r_{ij}}{\sigma_{ij}}\left(1-\frac{r_{ij}}{\sigma_i j}\right)\right\rangle_{ij} \tag{4.47}$$

$$= \frac{2\varphi Z}{d}\left\langle \frac{-r_{ij}V'(r_{ij})}{\sigma_{ij}^2V''(r_{ij}}\right\rangle_{ij} \tag{4.48}$$

$$\approx 2\frac{\varphi_{\mathrm{J}}}{d-1}e. \tag{4.49}$$

Thus, our better-fitting form for the $z-P$ relationship amounts to the statement that

$$\frac{\Delta z}{2d} = \hat{C}_\varphi\sqrt{\frac{d}{d-1}}\sqrt{e}. \tag{4.50}$$

Thus our scaling forms agree with the statement of reference [72] in the infinite-d limit, although we see better fit with our form in low dimensions.

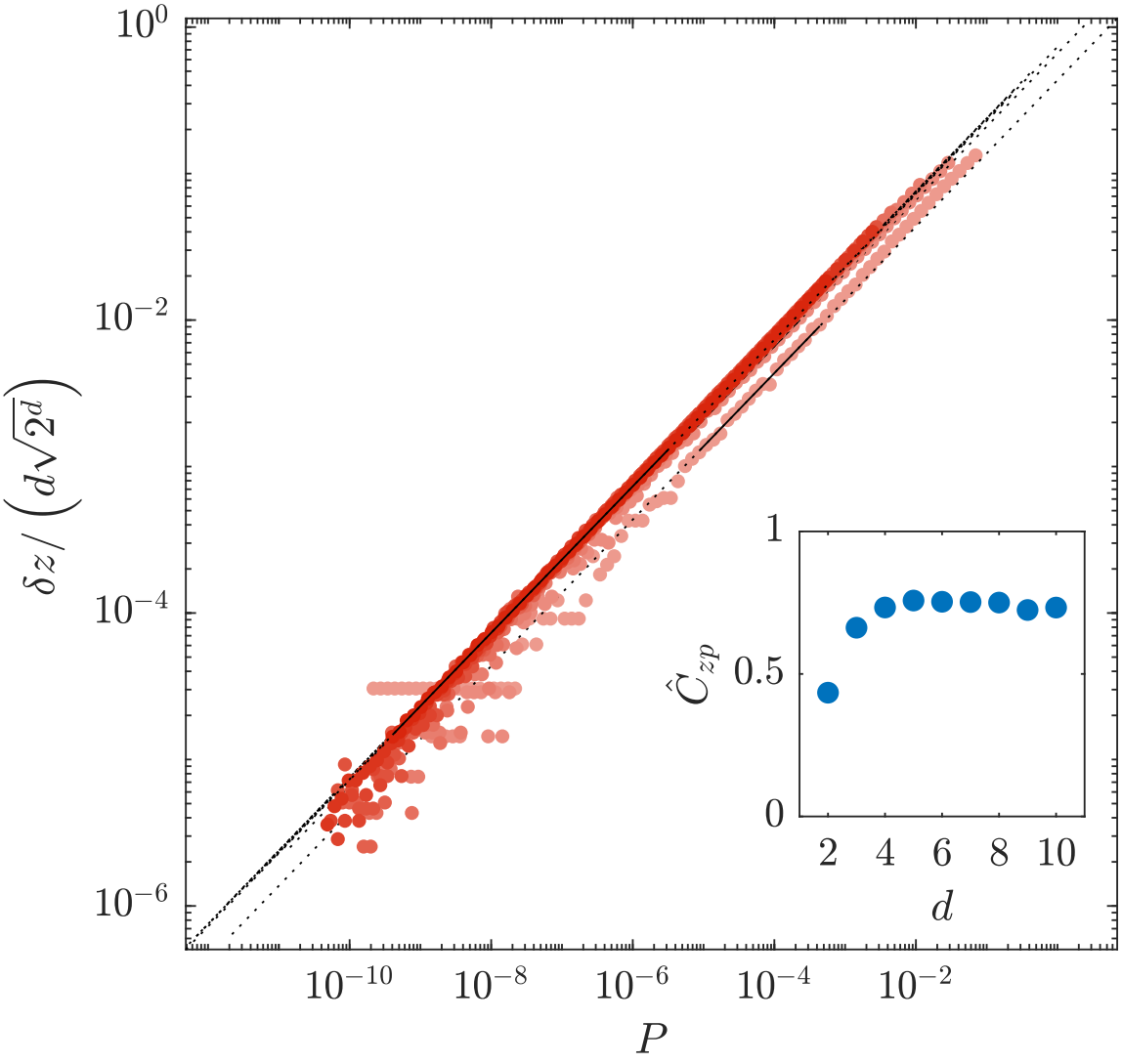

FIGURE 16. Scaled excess contacts scales with the square root of pressure as in figure 12. However, with excess contacts scaled by the expected mean field prediction, eqn. 4.7, the data collapse onto a single line. The inset confirms the collapse, showing $\hat{C}_{zp}$ to be nearly constant.

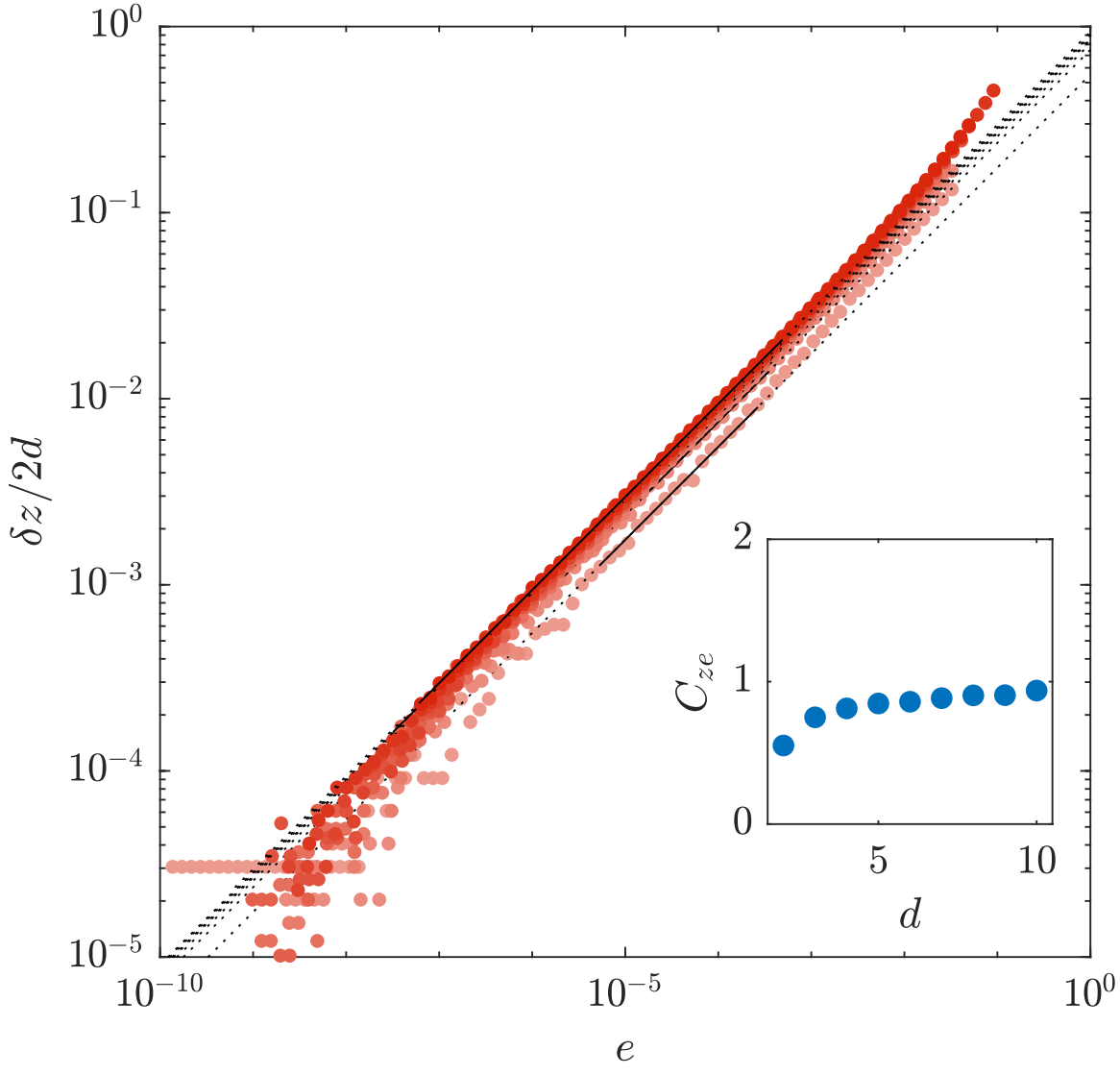

FIGURE 17. Scaled excess contacts scales with the square root of prestress for systems from $d = 2$ to $d = 10$. Black lines show the fits for C_{ze} using eqn 4.44. The fits ignore high and low pressure data as in figure 12. Lower inset shows the measured values of C_{ze} which have a clear upward trend.

CHAPTER V

CONCLUSION

While previous discussion of the Force Network Ensemble had been abstractly defined as a particular region in force space, our work in Chapter II was the first to measure this space in a concrete way. Moreover, we were able to connect our measurements of the Force Network Ensemble with a bulk measurement of angoricity. In doing so we not only discovered a new quantity, h_f which sets the scale of discretization for these systems, but also put the concept of angoricity on firm footing as a thermodynamic quantity. This connects thermodynamic approaches to granular materials with an underlying statistical mechanics, contributing to a complete statistical mechanical description of granular materials.

In Chapter III we expanded on this work, using the Force Network Ensemble to identify systems at the boundaries of available force space. From this we devised a provably correct first principles method for analytically identifying the only locations at which any contact change can occur under decompression. These force network defects are a completely new form of defect in amorphous materials and provide a framework for a ground up understanding of amorphous materials.

Despite the quantity of questions which have been answered by this work, an even greater number of interesting new questions have been raised. We hope that our approach of studying the space of allowed force configurations in granular systems serves as the foundation for future research. In particular, it would be interesting to use our strategy from Chapter III to predict contact breaking events in systems further from jamming via the Force Network Ensemble. While we limited our study to 2SSS systems, the same principle should apply to systems with more states of self stress. The problem becomes more challenging as the dimensionality of the space of states of self stress increases, but the same protocol can be used on a system with many states of self stress to predict not just the breakable contacts, but also all of the allowed 1SSS final configurations after decompression. Of course, since some contact breaking events are rearrangements, predictions for sequential contact breaking events will be less accurate. However, since about 86% of contact network changes are stable contact network changes, we would still expect to have decent predictive power for at least a few contact breaks [45, 46].

Another interesting and unexplored avenue is the search for force network defects in ultrastable systems [77–79], which have more contacts near jamming than random packings, and as such the defects may be delocalized or poorly defined. One could also attempt to modify our protocol to identify force network defects under shear rather than decompression. This would be especially interesting because the majority of the work done on soft spots has been conducted under shear, as were the recent studies which distinguished and quantified rearrangements versus stable contact network changes [45, 46].

Finally, one can also envision attempting to ascertain which force network defects will be rearrangements versus stable contact network changes. This could concievably be done with machine learning, in a similar fashion to much of the soft spots literature. Perhaps only the force network defects which exist within identifiable soft spots tend to lead to rearrangements, and others tend to lead to stable contact network changes.

In Chapter IV we took highly precise measurements of jamming scaling laws to measure the prefactors to jamming scaling relations. We showed that the mean field prediction is accurate for not just scaling exponents, but even the prefactors to these scaling laws. This was quite surprising because we expect these prefactors to be nonuniversal and highly sensitive to finite dimensional corrections to mean field theory. We were additionally able to show a first principles proof for the scaling prefactor between pressure and packing fraction. This showed that the mean field assumption was not necessary for that particular relation, and suggests that other relations may similarly be proven without the need for mean field theory. This calls into question the necessity of the mean field assumption in general for glasses and jamming. In particular, is there a derivation for the prefactor between excess contacts and pressure that does not rely on the mean field assumption? Moreover, are other scaling prefactors well predicted by the mean field? Of course, we do not expect that all useful results from the mean field may be proven without the mean field assumption - but perhaps more can be than previously thought.

The work presented in this dissertation represents a substantial addition to the literature regarding the Force Network Ensemble for jammed amorphous systems. We have shown two new methods by which the Force Network Ensemble can be used to better understand granular systems. Additionally we have shown that jamming scaling laws can be proven from first

principles without the mean field assumption, suggesting that the mean field assumption may not be necessary for understanding scaling laws in jamming.

REFERENCES CITED

[1] Johannes Kepler. Strena Seu de Nive Sexangula, 1611. URL https://www.goodreads.com/book/show/27591698-strena-seu-de-nive-sexangula.

[2] Thomas C. Hales. An overview of the Kepler conjecture. *arXiv:math/9811071*, November 1998. URL http://arxiv.org/abs/math/9811071. arXiv: math/9811071 version: 1.

[3] Roelof Louw. Soul City (Pyramid of Oranges), 1967. URL https://www.tate.org.uk/art/artworks/louw-soul-city-pyramid-of-oranges-t13881. Section: Art & artists.

[4] Jen Gunter. Photo by Jen Gunter on Unsplash, January 2021. URL https://unsplash.com/photos/A4BBdJQu2co.

[5] Corey S. O'Hern, Leonardo E. Silbert, Andrea J. Liu, and Sidney R. Nagel. Jamming at zero temperature and zero applied stress: The epitome of disorder. *Physical Review E*, 68(1), July 2003. ISSN 1063-651X, 1095-3787. doi: 10.1103/PhysRevE.68.011306. URL https://link.aps.org/doi/10.1103/PhysRevE.68.011306.

[6] Carl P. Goodrich, Andrea J. Liu, and James P. Sethna. Scaling ansatz for the jamming transition. *Proceedings of the National Academy of Sciences*, 113(35):9745–9750, August 2016. ISSN 0027-8424, 1091-6490. doi: 10.1073/pnas.1601858113. URL http://www.pnas.org/lookup/doi/10.1073/pnas.1601858113.

[7] S.F. Edwards and R.B.S. Oakeshott. Theory of powders. *Physica A: Statistical Mechanics and its Applications*, 157(3):1080–1090, June 1989. ISSN 03784371. doi: 10.1016/0378-4371(89)90034-4. URL http://linkinghub.elsevier.com/retrieve/pii/0378437189900344.

[8] Sam F Edwards. The distribution of forces in a granular system under external stress is a spinglass problem. *Journal of Physics A: Mathematical and Theoretical*, 41(32):324019, August 2008. ISSN 1751-8113, 1751-8121. doi: 10.1088/1751-8113/41/32/324019. URL http://stacks.iop.org/1751-8121/41/i=32/a=324019?key=crossref.91301149080e11e0fb4cc0316f09b324.

[9] Dapeng Bi, Silke Henkes, Karen E. Daniels, and Bulbul Chakraborty. The Statistical Physics of Athermal Materials. *Annual Review of Condensed Matter Physics*, 6(1):63–83, March 2015. ISSN 1947-5454, 1947-5462. doi: 10.1146/annurev-conmatphys-031214-014336. URL http://arxiv.org/abs/1404.1854. arXiv: 1404.1854.

[10] Jacco H. Snoeijer, Thijs J. H. Vlugt, Martin van Hecke, and Wim van Saarloos. Force Network Ensemble: A New Approach to Static Granular Matter. *Physical Review Letters*, 92(5), February 2004. ISSN 0031-9007, 1079-7114. doi: 10.1103/PhysRevLett.92.054302. URL https://link.aps.org/doi/10.1103/PhysRevLett.92.054302.

[11] Brian P. Tighe, Jacco H. Snoeijer, Thijs J. H. Vlugt, and Martin van Hecke. The force network ensemble for granular packings. *Soft Matter*, 6(13):2908, 2010. ISSN 1744-683X, 1744-6848. doi: 10.1039/b926592a. URL http://xlink.rsc.org/?DOI=b926592a.

[12] James D. Sartor and Eric I. Corwin. Direct measurement of force configurational entropy in jamming. *Physical Review E*, 101(5), May 2020. ISSN 2470-0045, 2470-0053. doi: 10.1103/PhysRevE.101.050902. URL https://link.aps.org/doi/10.1103/PhysRevE.101.050902.

[13] James D. Sartor and Eric I. Corwin. Predicting Defects in Soft Sphere Packings Near Jamming Using The Force Network Ensemble. *arXiv:2108.09385 [cond-mat]*, September 2021. URL http://arxiv.org/abs/2108.09385. arXiv: 2108.09385.

[14] James D. Sartor, Sean A. Ridout, and Eric I. Corwin. Mean-Field Predictions of Scaling Prefactors Match Low-Dimensional Jammed Packings. *Physical Review Letters*, 126(4): 048001, January 2021. doi: 10.1103/PhysRevLett.126.048001. URL https://link.aps.org/doi/10.1103/PhysRevLett.126.048001.

[15] James G. Puckett and Karen E. Daniels. Equilibrating Temperaturelike Variables in Jammed Granular Subsystems. *Physical Review Letters*, 110(5):058001, January 2013. ISSN 0031-9007, 1079-7114. doi: 10.1103/PhysRevLett.110.058001. URL https://link.aps.org/doi/10.1103/PhysRevLett.110.058001.

[16] Ephraim S. Bililign, Jonathan E. Kollmer, and Karen E. Daniels. Protocol Dependence and State Variables in the Force-Moment Ensemble. *Physical Review Letters*, 122(3):038001, January 2019. ISSN 0031-9007, 1079-7114. doi: 10.1103/PhysRevLett.122.038001. URL https://link.aps.org/doi/10.1103/PhysRevLett.122.038001.

[17] Walter Grimus. 100th anniversary of the Sackur–Tetrode equation. *Annalen der Physik*, 525 (3):A32–A35, 2013. ISSN 1521-3889. doi: 10.1002/andp.201300720. URL https://onlinelibrary.wiley.com/doi/abs/10.1002/andp.201300720.

[18] H. Tetrode. Die chemische Konstante der Gase und das elementare Wirkungsquantum. *Annalen der Physik*, 343(7):434–442, January 1912. ISSN 1521-3889. doi: 10.1002/andp.19123430708. URL https://onlinelibrary.wiley.com/doi/abs/10.1002/andp.19123430708.

[19] S. F. Edwards and D. V. Grinev. Granular materials: Towards the statistical mechanics of jammed configurations. *Advances in Physics*, 51(8):1669–1684, December 2002. ISSN 0001-8732, 1460-6976. doi: 10.1080/0001873021000030780. URL http://www.tandfonline.com/doi/abs/10.1080/0001873021000030780.

[20] S. Henkes and B. Chakraborty. A statistical mechanics framework for static granular matter. *Physical Review E*, 79(6), June 2009. ISSN 1539-3755, 1550-2376. doi: 10.1103/PhysRevE.79.061301. URL http://arxiv.org/abs/0810.5715. arXiv: 0810.5715.

[21] Patrick Charbonneau, Eric I. Corwin, Giorgio Parisi, and Francesco Zamponi. Universal Microstructure and Mechanical Stability of Jammed Packings. *Physical Review Letters*, 109 (20), November 2012. ISSN 0031-9007, 1079-7114. doi: 10.1103/PhysRevLett.109.205501. URL https://link.aps.org/doi/10.1103/PhysRevLett.109.205501.

[22] Erik Bitzek, Pekka Koskinen, Franz Gähler, Michael Moseler, and Peter Gumbsch. Structural Relaxation Made Simple. *Physical Review Letters*, 97(17), October 2006. ISSN 0031-9007, 1079-7114. doi: 10.1103/PhysRevLett.97.170201. URL https://link.aps.org/doi/10.1103/PhysRevLett.97.170201.

[23] Patrick Charbonneau, Eric I. Corwin, Giorgio Parisi, and Francesco Zamponi. Jamming Criticality Revealed by Removing Localized Buckling Excitations. *Physical Review Letters*, 114(12), March 2015. ISSN 0031-9007, 1079-7114. doi: 10.1103/PhysRevLett.114.125504. URL https://link.aps.org/doi/10.1103/PhysRevLett.114.125504.

[24] Wouter G. Ellenbroek, Varda F. Hagh, Avishek Kumar, M.F. Thorpe, and Martin van Hecke. Rigidity Loss in Disordered Systems: Three Scenarios. *Physical Review Letters*, 114(13), April 2015. ISSN 0031-9007, 1079-7114. doi: 10.1103/PhysRevLett.114.135501. URL https://link.aps.org/doi/10.1103/PhysRevLett.114.135501.

[25] Varda F. Hagh, Eric I. Corwin, Kenneth Stephenson, and M. F. Thorpe. A broader view on jamming: from spring networks to circle packings. *Soft Matter*, 15(15):3076–3084, 2019. ISSN 1744-683X, 1744-6848. doi: 10.1039/C8SM01768A. URL http://xlink.rsc.org/?DOI=C8SM01768A.

[26] Simon Dagois-Bohy, Brian P. Tighe, Johannes Simon, Silke Henkes, and Martin van Hecke. Soft-Sphere Packings at Finite Pressure but Unstable to Shear. *Physical Review Letters*, 109(9), August 2012. ISSN 0031-9007, 1079-7114. doi: 10.1103/PhysRevLett.109.095703. URL https://link.aps.org/doi/10.1103/PhysRevLett.109.095703.

[27] Carl P. Goodrich, Andrea J. Liu, and Sidney R. Nagel. Finite-Size Scaling at the Jamming Transition. *Physical Review Letters*, 109(9), August 2012. ISSN 0031-9007, 1079-7114. doi: 10.1103/PhysRevLett.109.095704. URL https://link.aps.org/doi/10.1103/PhysRevLett.109.095704.

[28] Brian P Tighe and Thijs J H Vlugt. Stress fluctuations in granular force networks. *Journal of Statistical Mechanics: Theory and Experiment*, 2011(04):P04002, April 2011. ISSN 1742-5468. doi: 10.1088/1742-5468/2011/04/P04002. URL http://stacks.iop.org/1742-5468/2011/i=04/a=P04002?key=crossref.ec4d93d62266e3242532ceb8b8079f6f.

[29] C. Bradford Barber, David P. Dobkin, and Hannu Huhdanpaa. The quickhull algorithm for convex hulls. *ACM Transactions on Mathematical Software*, 22(4):469–483, December 1996. ISSN 00983500. doi: 10.1145/235815.235821. URL http://portal.acm.org/citation.cfm?doid=235815.235821.

[30] M Mailman and Bulbul Chakraborty. Using point-to-set correlations to probe unjamming of frictionless grains. *Journal of Statistical Mechanics-theory and Experiment - J STAT MECH-THEORY EXP*, 2012, May 2012. doi: 10.1088/1742-5468/2012/05/P05001.

[31] Charles H Bennett. Efficient estimation of free energy differences from Monte Carlo data. *Journal of Computational Physics*, 22(2):245–268, October 1976. ISSN 00219991. doi: 10.1016/0021-9991(76)90078-4. URL https://linkinghub.elsevier.com/retrieve/pii/0021999176900784.

[32] Sean McNamara, Patrick Richard, Sébastien Kiesgen de Richter, Gérard Le Caër, and Renaud Delannay. Measurement of granular entropy. *Physical Review E*, 80(3), September 2009. ISSN 1539-3755, 1550-2376. doi: 10.1103/PhysRevE.80.031301. URL https://link.aps.org/doi/10.1103/PhysRevE.80.031301.

[33] G Taylor. The mechanism of plastic deformation of crystals. Part I.—Theoretical. *Proceedings of the Royal Society of London. Series A, Containing Papers of a Mathematical and Physical Character*, 145(855):362–387, July 1934. ISSN 0950-1207, 2053-9150. doi: 10.1098/rspa.1934.0106. URL https://royalsocietypublishing.org/doi/10.1098/rspa.1934.0106.

[34] Carl P. Goodrich, Andrea J. Liu, and Sidney R. Nagel. Solids between the mechanical extremes of order and disorder. *Nature Physics*, 10(8):578–581, August 2014. ISSN 1745-2473, 1745-2481. doi: 10.1038/nphys3006. URL http://www.nature.com/articles/nphys3006.

[35] M. L. Manning and A. J. Liu. Vibrational Modes Identify Soft Spots in a Sheared Disordered Packing. *Physical Review Letters*, 107(10):108302, August 2011. ISSN 0031-9007, 1079-7114. doi: 10.1103/PhysRevLett.107.108302. URL https://link.aps.org/doi/10.1103/PhysRevLett.107.108302.

[36] E.D. Cubuk, S.S. Schoenholz, J.M. Rieser, B.D. Malone, J. Rottler, D.J. Durian, E. Kaxiras, and A.J. Liu. Identifying Structural Flow Defects in Disordered Solids Using Machine-Learning Methods. *Physical Review Letters*, 114(10):108001, March 2015. ISSN 0031-9007, 1079-7114. doi: 10.1103/PhysRevLett.114.108001. URL https://link.aps.org/doi/10.1103/PhysRevLett.114.108001.

[37] Ekin D. Cubuk, Samuel S. Schoenholz, Efthimios Kaxiras, and Andrea J. Liu. Structural Properties of Defects in Glassy Liquids. *The Journal of Physical Chemistry B*, 120(26): 6139–6146, July 2016. ISSN 1520-6106, 1520-5207. doi: 10.1021/acs.jpcb.6b02144. URL https://pubs.acs.org/doi/10.1021/acs.jpcb.6b02144.

[38] Jun Ding, Sylvain Patinet, Michael L. Falk, Yongqiang Cheng, and Evan Ma. Soft spots and their structural signature in a metallic glass. *Proceedings of the National Academy of Sciences*, 111(39):14052–14056, September 2014. ISSN 0027-8424, 1091-6490. doi: 10.1073/pnas.1412095111. URL http://www.pnas.org/lookup/doi/10.1073/pnas.1412095111.

[39] Sven Wijtmans and M. Lisa Manning. Disentangling defects and sound modes in disordered solids. *Soft Matter*, 13(34):5649–5655, 2017. ISSN 1744-683X, 1744-6848. doi: 10.1039/C7SM00792B. URL http://xlink.rsc.org/?DOI=C7SM00792B.

[40] S. S. Schoenholz, E. D. Cubuk, D. M. Sussman, E. Kaxiras, and A. J. Liu. A structural approach to relaxation in glassy liquids. *Nature Physics*, 12(5):469–471, May 2016. ISSN 1745-2473, 1745-2481. doi: 10.1038/nphys3644. URL http://www.nature.com/articles/nphys3644.

[41] S S Schoenholz, A J Liu, R A Riggleman, and J Rottler. Understanding Plastic Deformation in Thermal Glasses from Single-Soft-Spot Dynamics. page 11, 2014.

[42] D. Richard, M. Ozawa, S. Patinet, E. Stanifer, B. Shang, S. A. Ridout, B. Xu, G. Zhang, P. K. Morse, J.-L. Barrat, L. Berthier, M. L. Falk, P. Guan, A. J. Liu, K. Martens, S. Sastry, D. Vandembroucq, E. Lerner, and M. L. Manning. Predicting plasticity in disordered solids from structural indicators. *Physical Review Materials*, 4(11):113609, November 2020. ISSN 2475-9953. doi: 10.1103/PhysRevMaterials.4.113609. URL https://link.aps.org/doi/10.1103/PhysRevMaterials.4.113609.

[43] Jason W. Rocks, Sean A. Ridout, and Andrea J. Liu. Learning-based approach to plasticity in athermal sheared amorphous packings: Improving softness. *APL Materials*, 9(2):021107, February 2021. ISSN 2166-532X. doi: 10.1063/5.0035395. URL https://aip.scitation.org/doi/10.1063/5.0035395.

[44] Sean A. Ridout, Jason W. Rocks, and Andrea J. Liu. Correlation of plastic events with local structure in jammed packings across spatial dimensions. *arXiv:2011.13049 [cond-mat]*, November 2020. URL http://arxiv.org/abs/2011.13049. arXiv: 2011.13049.

[45] Peter Morse, Sven Wijtmans, Merlijn van Deen, Martin van Hecke, and M. Lisa Manning. Differences in plasticity between hard and soft spheres. *Physical Review Research*, 2(2): 023179, May 2020. ISSN 2643-1564. doi: 10.1103/PhysRevResearch.2.023179. URL https://link.aps.org/doi/10.1103/PhysRevResearch.2.023179.

[46] Philip J. Tuckman, Kyle VanderWerf, Ye Yuan, Shiyun Zhang, Jerry Zhang, Mark D. Shattuck, and Corey S. O'Hern. Contact network changes in ordered and disordered disk packings. *Soft Matter*, 16(41):9443–9455, 2020. ISSN 1744-683X, 1744-6848. doi: 10.1039/D0SM01137A. URL http://xlink.rsc.org/?DOI=D0SM01137A.

[47] James Clerk Maxwell. On the calculation of the equilibrium and stiffness of frames. *The London, Edinburgh, and Dublin Philosophical Magazine and Journal of Science*, 27(182): 294–299, 1864. doi: 10.1017/CBO9780511698095. URL http://ebooks.cambridge.org/ref/id/CBO9780511698095.

[48] Peter K. Morse and Eric I. Corwin. Echoes of the Glass Transition in Athermal Soft Spheres. *Physical Review Letters*, 119(11):118003, September 2017. ISSN 0031-9007, 1079-7114. doi: 10.1103/PhysRevLett.119.118003. URL https://link.aps.org/doi/10.1103/PhysRevLett.119.118003.

[49] Camille Jordan. Essai sur la géométrie à n dimensions. *Bulletin de la Société mathématique de France*, 2:103–174, 1875. ISSN 0037-9484, 2102-622X. doi: 10.24033/bsmf.90. URL http://www.numdam.org/item?id=BSMF_1875__3__103_2.

[50] Daniel M. Sussman, Carl P. Goodrich, and Andrea J. Liu. Spatial structure of states of self stress in jammed systems. *Soft Matter*, 12(17):3982–3990, 2016. ISSN 1744-683X, 1744-6848. doi: 10.1039/C6SM00094K. URL http://xlink.rsc.org/?DOI=C6SM00094K.

[51] Andrea J. Liu and Sidney R. Nagel. The Jamming Transition and the Marginally Jammed Solid. *Annual Review of Condensed Matter Physics*, 1(1):347–369, August 2010. ISSN 1947-5454, 1947-5462. doi: 10.1146/annurev-conmatphys-070909-104045. URL http://www.annualreviews.org/doi/10.1146/annurev-conmatphys-070909-104045.

[52] Patrick Charbonneau, Jorge Kurchan, Giorgio Parisi, Pierfrancesco Urbani, and Francesco Zamponi. Glass and Jamming Transitions: From Exact Results to Finite-Dimensional Descriptions. *Annual Review of Condensed Matter Physics*, 8(1):265–288, March 2017. ISSN 1947-5454, 1947-5462. doi: 10.1146/annurev-conmatphys-031016-025334. URL http://www.annualreviews.org/doi/10.1146/annurev-conmatphys-031016-025334.

[53] Giorgio Parisi and Francesco Zamponi. Mean-field theory of hard sphere glasses and jamming. *Reviews of Modern Physics*, 82(1):789–845, March 2010. ISSN 0034-6861, 1539-0756. doi: 10.1103/RevModPhys.82.789. URL https://link.aps.org/doi/10.1103/RevModPhys.82.789.

[54] Giorgio Parisi, Pierfrancesco Urbani, and Francesco Zamponi. *Theory of Simple Glasses: Exact Solutions in Infinite Dimensions*. Cambridge University Press, New York, February 2020. ISBN 978-1-107-19107-5.

[55] Giorgio Parisi, Yoav G. Pollack, Itamar Procaccia, Corrado Rainone, and Murari Singh. Robustness of mean field theory for hard sphere models. *Physical Review E*, 97(6), June 2018. ISSN 2470-0045, 2470-0053. doi: 10.1103/PhysRevE.97.063003. URL https://link.aps.org/doi/10.1103/PhysRevE.97.063003.

[56] Corey S. O'Hern, Stephen A. Langer, Andrea J. Liu, and Sidney R. Nagel. Random Packings of Frictionless Particles. *Physical Review Letters*, 88(7), January 2002. ISSN 0031-9007, 1079-7114. doi: 10.1103/PhysRevLett.88.075507. URL https://link.aps.org/doi/10.1103/PhysRevLett.88.075507.

[57] Patrick Charbonneau, Eric I. Corwin, Giorgio Parisi, Alexis Poncet, and Francesco Zamponi. Universal Non-Debye Scaling in the Density of States of Amorphous Solids. *Physical Review Letters*, 117(4), July 2016. ISSN 0031-9007, 1079-7114. doi: 10.1103/PhysRevLett.117.045503. URL https://link.aps.org/doi/10.1103/PhysRevLett.117.045503.

[58] Ludovic Berthier, Giulio Biroli, Patrick Charbonneau, Eric I. Corwin, Silvio Franz, and Francesco Zamponi. Perspective: Gardner Physics in Amorphous Solids and Beyond. *The Journal of Chemical Physics*, 151(1):010901, July 2019. ISSN 0021-9606, 1089-7690. doi: 10.1063/1.5097175. URL `http://arxiv.org/abs/1902.10494`. arXiv: 1902.10494.

[59] R.C. Dennis and E.I. Corwin. Jamming Energy Landscape is Hierarchical and Ultrametric. *Physical Review Letters*, 124(7), February 2020. ISSN 0031-9007, 1079-7114. doi: 10.1103/PhysRevLett.124.078002. URL `https://link.aps.org/doi/10.1103/PhysRevLett.124.078002`.

[60] Francesco Arceri and Eric I. Corwin. Vibrational properties of hard and soft spheres are unified at jamming. *arXiv:1912.05697 [cond-mat]*, December 2019. URL `http://arxiv.org/abs/1912.05697`. arXiv: 1912.05697.

[61] M. P. Allen, M. P. Allen, D. J. Tildesley, TILDESLEY ALLEN, and D. J. Tildesley. *Computer Simulation of Liquids*. Clarendon Press, 1989. ISBN 978-0-19-855645-9.

[62] Matthieu Wyart, Leonardo E. Silbert, Sidney R. Nagel, and Thomas A. Witten. Effects of compression on the vibrational modes of marginally jammed solids. *Physical Review E*, 72 (5), November 2005. ISSN 1539-3755, 1550-2376. doi: 10.1103/PhysRevE.72.051306. URL `https://link.aps.org/doi/10.1103/PhysRevE.72.051306`.

[63] M. Wyart. On the rigidity of amorphous solids. *Annales de Physique*, 30(3):1–96, 2005. ISSN 0003-4169, 1286-4838. doi: 10.1051/anphys:2006003. URL `http://www.annphys.org/10.1051/anphys:2006003`.

[64] Alessio Zaccone and Enzo Scossa-Romano. Approximate analytical description of the nonaffine response of amorphous solids. *Physical Review B*, 83(18), May 2011. ISSN 1098-0121, 1550-235X. doi: 10.1103/PhysRevB.83.184205. URL `https://link.aps.org/doi/10.1103/PhysRevB.83.184205`.

[65] Danilo B. Liarte, Xiaoming Mao, Olaf Stenull, and T.C. Lubensky. Jamming as a Multicritical Point. *Physical Review Letters*, 122(12), March 2019. ISSN 0031-9007, 1079-7114. doi: 10.1103/PhysRevLett.122.128006. URL `https://link.aps.org/doi/10.1103/PhysRevLett.122.128006`.

[66] Silvio Franz, Giorgio Parisi, Maxime Sevelev, Pierfrancesco Urbani, and Francesco Zamponi. Universality of the SAT-UNSAT (jamming) threshold in non-convex continuous constraint satisfaction problems. *SciPost Physics*, 2(3), June 2017. ISSN 2542-4653. doi: 10.21468/SciPostPhys.2.3.019. URL `https://scipost.org/10.21468/SciPostPhys.2.3.019`.

[67] J A Aronovitz and M J Stephen. Universal features of the shapes of percolation clusters and lattice animals. *Journal of Physics A: Mathematical and General*, 20(9):2539–2556, June 1987. ISSN 0305-4470, 1361-6447. doi: 10.1088/0305-4470/20/9/038. URL `https://iopscience.iop.org/article/10.1088/0305-4470/20/9/038`.

[68] V Privman, P. C. Hohenberg, and A Aharony. *Universal Critical-Point Amplitude Relations, in "Phase transition and critical phenomena" vol. 14, C. Domb and JL Lebowitz eds.* Academic Press, 1991.

[69] E Brizin and J Zinn-Justin. Finite size effects in phase transitions. *Nuclear Physics B*, 257:27, 1985. doi: 10.1016/0550-3213(85)90379-7.

[70] Giorgio Parisi and Juan J. Ruiz-Lorenzo. Scaling above the upper critical dimension in Ising models. *Physical Review B*, 54(6):R3698–R3701, August 1996. ISSN 0163-1829, 1095-3795. doi: 10.1103/PhysRevB.54.R3698. URL https://link.aps.org/doi/10.1103/PhysRevB.54.R3698.

[71] H. W. J Blöte and E Luijten. Universality and the five-dimensional Ising model. *Europhysics Letters (EPL)*, 38(8):565–570, June 1997. ISSN 0295-5075, 1286-4854. doi: 10.1209/epl/i1997-00284-x. URL https://iopscience.iop.org/article/10.1209/epl/i1997-00284-x.

[72] Masanari Shimada, Hideyuki Mizuno, Ludovic Berthier, and Atsushi Ikeda. Low-frequency vibrations of jammed packings in large spatial dimensions. *arXiv:1910.07238 [cond-mat]*, October 2019. URL http://arxiv.org/abs/1910.07238. arXiv: 1910.07238.

[73] Meng Fan, Kai Zhang, Jan Schroers, Mark D. Shattuck, and Corey S. O'Hern. Particle rearrangement and softening contributions to the nonlinear mechanical response of glasses. *Physical Review E*, 96(3), September 2017. ISSN 2470-0045, 2470-0053. doi: 10.1103/PhysRevE.96.032602. URL https://link.aps.org/doi/10.1103/PhysRevE.96.032602.

[74] S. Pellegrino. Structural computations with the singular value decomposition of the equilibrium matrix. *International Journal of Solids and Structures*, 30(21):3025–3035, January 1993. ISSN 0020-7683. doi: 10.1016/0020-7683(93)90210-X. URL http://www.sciencedirect.com/science/article/pii/002076839390210X.

[75] T C Lubensky, C L Kane, Xiaoming Mao, A Souslov, and Kai Sun. Phonons and elasticity in critically coordinated lattices. *Reports on Progress in Physics*, 78(7):073901, July 2015. ISSN 0034-4885, 1361-6633. doi: 10.1088/0034-4885/78/7/073901. URL http://stacks.iop.org/0034-4885/78/i=7/a=073901?key=crossref.ed7e2e7f699a1e53049f16f3a85fc3dc.

[76] Daniel M. Mueth, Heinrich M. Jaeger, and Sidney R. Nagel. Force distribution in a granular medium. *Physical Review E*, 57(3):3164–3169, March 1998. ISSN 1063-651X, 1095-3787. doi: 10.1103/PhysRevE.57.3164. URL https://link.aps.org/doi/10.1103/PhysRevE.57.3164.

[77] Geert Kapteijns, Wencheng Ji, Carolina Brito, Matthieu Wyart, and Edan Lerner. Fast generation of ultrastable computer glasses by minimization of an augmented potential energy. *Physical Review E*, 99(1):012106, January 2019. ISSN 2470-0045, 2470-0053. doi: 10.1103/PhysRevE.99.012106. URL https://link.aps.org/doi/10.1103/PhysRevE.99.012106.

[78] Varda F. Hagh, Sidney R. Nagel, Andrea J. Liu, M. Lisa Manning, and Eric I. Corwin. Transient degrees of freedom and stability. *arXiv:2105.10846 [cond-mat]*, May 2021. URL http://arxiv.org/abs/2105.10846. arXiv: 2105.10846.

[79] Andrea Ninarello, Ludovic Berthier, and Daniele Coslovich. Models and Algorithms for the Next Generation of Glass Transition Studies. *Physical Review X*, 7(2):021039, June 2017. ISSN 2160-3308. doi: 10.1103/PhysRevX.7.021039. URL http://link.aps.org/doi/10.1103/PhysRevX.7.021039.